

THE

Journal

OF THE AMERICAN
LEATHER CHEMISTS ASSOCIATION

May 2021

Vol. CXVI, No.5

JALCA 116(5), 145-184, 2021



116th Annual Convention

to be held at the
Eaglewood Resort & Spa
1401 Nordic Road
Itasca, IL 60143

DATE CHANGE:
June 21-24, 2022

For more information go to:
[leatherchemists.org/
annual_convention.asp](http://leatherchemists.org/annual_convention.asp)

Contents

Collagen Fiber Opening of Cattle Hides in Urea/Calcium Hydroxide Solutions by Qian Zhang, Jie Liu, Xiumin Li, Hui Liu, Yadi Hu and Keyong Tang	147
Oxidized Maltodextrin: A Novel Ligand for Aluminum-Zirconium Complex Tanning by Xueru Guo, Yue Yu, Ya-nan Wang and Bi Shiv	155
Effects of a Clean Subcritical Degreasing System on Wool Fibers by Qiao Xia, Yinxuan Wang, Meina Zhang, Zongcai Zhang and Hong Dai	162
Learning to Recognize Irregular Features on Leather Surfaces by Masood Aslam, Tariq M. Khan, Syed Saud Naqvi, Geoff Holmes and Rafea Naffa	169
Lifelines	179
ACLA News Obituary	184

Distributed by



An imprint of the University of Cincinnati Press

ISSN: 0002-9726

Communications for Journal Publication

Manuscripts, Technical Notes and Trade News Releases should contact:
MR. STEVEN D. LANGE, Journal Editor, 1314 50th Street, Suite 103, Lubbock, TX 79412, USA
E-mail: jalcaeditor@gmail.com Mobile phone: (814) 414-5689

Contributors should consult the Journal Publication Policy at:
http://www.leatherchemists.org/journal_publication_policy.asp

Beamhouse efficiency takes perfect balance.

Making leather on time, on spec and within budget requires a careful balance of chemistry and process. Buckman enables tanneries to master that balance with our comprehensive Beamhouse & Tanyard Systems. They include advanced chemistries that not only protect the hide but also maximize the effectiveness of each process, level out the differences in raw materials and reduce variations in batch processing. The result is cleaner, flatter pelts. More uniform characteristics. And improved area yield.

In addition, we offer unsurpassed expertise and technical support to help solve processing problems and reduce environmental impact with chemistries that penetrate faster, save processing time, improve effluent and enhance safety.

With Buckman Beamhouse & Tanyard Systems, tanneries can get more consistent quality and more consistent savings. Maintain the perfect balance. Connect with a Buckman representative or visit us at Buckman.com.

1945
2020 **Buckman75**

JOURNAL OF THE AMERICAN LEATHER CHEMISTS ASSOCIATION

*Proceedings, Reports, Notices, and News
of the*
AMERICAN LEATHER CHEMISTS ASSOCIATION

OFFICERS

MIKE BLEY, *President*
Eagle Ottawa – Lear
2930 Auburn Road
Rochester Hills, MI 48309

JOSEPH HOEFLER, *Vice-President*
The Dow Chemical Company
400 Arcola Rd.
Collegeville, PA 19426

COUNCILORS

Shawn Brown
Quaker Color
201 S. Hellertown Ave.
Quakertown, PA 18951

Steve Lange
Leather Research Laboratory
University of Cincinnati
5997 Center Hill Ave., Bldg. C
Cincinnati, OH 45224

John Rodden
Union Specialties, Inc.
3 Malcolm Hoyt Dr.
Newburyport, MA 01950

Jose Luis Gallegos
Elementis LTP
546 S. Water St.
Milwaukee, WI 53204

LeRoy Lehman
LANXESS Corporation
9501 Tallwood Dr.
Indian Trail, NC 28079

Marcelo Fraga de Sousa
Buckman North America
1256 N. McLean Blvd.
Memphis, TN 38108

EDITORIAL BOARD

Dr. Meral Birbir
Biology Department
Faculty of Arts and Sciences
Marmara University
Istanbul, Turkey

Chris Black
Consultant
St. Joseph, Missouri

Dr. Eleanor M. Brown
Eastern Regional
Research Center
U.S. Department of Agriculture
Wyndmoor, Pennsylvania

Kadir Donmez
Leather Research Laboratory
University of Cincinnati
Cincinnati, Ohio

Dr. Anton Ela'mma
Retired
Perkiomenville, Pennsylvania

Cietta Fambrough
Leather Research Laboratory
University of Cincinnati
Cincinnati, Ohio

Mainul Haque
ALCA Education
Committee Chairman
Rochester Hills, Michigan

Joseph Hoefler
Dow Chemical Company
Collegeville, Pennsylvania

Elton Hurlow
Buckman International
Memphis, Tennessee

Prasad V. Inaganti
Wickett and Craig of America
Curwensville, Pennsylvania

Dr. Tariq M. Khan
Research Fellow, Machine Learning
Faculty of Sci Eng & Built Env
School of Info Technology
Geelong Waurm Ponds Campus
Victoria, Australia

Nick Latona
Eastern Regional Research Center
U.S. Department of Agriculture
Wyndmoor, Pennsylvania

Dr. Xue-pin Liao
National Engineering Centre for Clean
Technology of Leather Manufacture
Sichuan University
Chengdu, China

Dr. Cheng-Kung Liu
Eastern Regional Research Center
U.S. Department of Agriculture
Wyndmoor, Pennsylvania

Dr. Rafea Naffa
New Zealand Leather & Shoe
Research Association Inc. (LASRA*)
Palmerston North, New Zealand

Edwin Nungesser
Dow Chemical Company
Collegeville, Pennsylvania

Dr. Benson Ongarora
Department of Chemistry
Dedan Kimathi University of Technology
Nyeri, Kenya

Lucas Paddock
Chemtan Company, Inc.
Exeter, New Hampshire

Dr. J. Raghava Rao
Central Leather
Research Institute
Chennai, India

Andreas W. Rhein
Tyson Foods, Inc.
Dakota Dunes, South Dakota

Dr. Majher Sarker
Eastern Regional
Research Center
U.S. Department of Agriculture
Wyndmoor, Pennsylvania

Dr. Bi Shi
National Engineering Laboratory
Sichuan University
Chengdu, China

Dr. Palanisamy Thanikaivelan
Central Leather
Research Institute
Chennai, India

Dr. Xiang Zhang
Genomics, Epigenomics and
Sequencing Core
University of Cincinnati
Cincinnati, Ohio

Dr. Luis A. Zugno
Buckman International
Memphis, Tennessee

PAST PRESIDENTS

G. A. KERR, W. H. TEAS, H. C. REED, J. H. YOCUM, F. H. SMALL, H. T. WILSON, J. H. RUSSELL, F. P. VEITCH, W. K. ALSOP, L. E. LEVI, C. R. OBERFELL, R. W. GRIFFITH, C. C. SMOOT, III, J. S. ROGERS, LLOYD BALDERSON, J. A. WILSON, R. W. FREY, G. D. McLAUGHLIN, FRED O'FLAHERTY, A. C. ORTHMANN, H. B. MERRILL, V. J. MLEJNEK, J. H. HIGHBERGER, DEAN WILLIAMS, T. F. OBERLANDER, A. H. WINHEIM, R. M. KOPPENHOEFER, H. G. TURLEY, E. S. FLINN, E. B. THORSTENSEN, M. MAESER, R. G. HENRICH, R. STUBBINGS, D. MEO, JR., R. M. LOLLAR, B. A. GROTA, M. H. BATTLES, J. NAGHSKI, T. C. THORSTENSEN, J. J. TANCOS, W. E. DOOLEY, J. M. CONSTANTIN, L. K. BARBER, J. J. TANCOS, W. C. PRENTISS, S. H. FAIRHELLER, M. SIEGLER, F. H. RUTLAND, D.G. BAILEY, R. A. LAUNDER, B. D. MILLER, G. W. HANSON, D. G. MORRISON, R. F. WHITE, E. L. HURLOW, M. M. TAYLOR, J. F. LEVY, D. T. DIDATO, R. HAMMOND, D. G. MORRISON, W. N. MULLINIX, D. C. SHELLY, W. N. MARMER, S. S. YANEK, D. LEBLANC, C.G. KEYSER, A.W. RHEIN, S. GILBERG, S. LANGE, S. DRAYNA, D. PETERS

THE JOURNAL OF THE AMERICAN LEATHER CHEMISTS ASSOCIATION (USPS #019-334) is published monthly by The American Leather Chemists Association, 1314 50th Street, Suite 103, Lubbock, Texas 79412. Telephone (806)744-1798 Fax (806)744-1785. Single copy price: \$8.50 members, \$17.00 non-member. Subscriptions: \$185 for hard copy plus postage and handling of \$60 for domestic subscribers and \$70 for foreign subscribers; \$185 for ezine only; and \$205 for hard copy and ezine plus postage and handling of \$60 for domestic subscribers and \$70 for foreign subscribers.

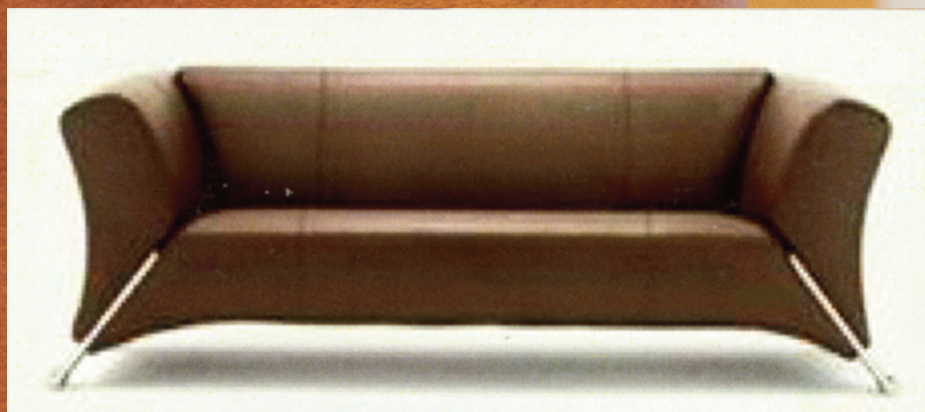
Periodical Postage paid at Lubbock, Texas and additional mailing offices. Postmaster send change of addresses to The American Leather Chemists Association, 1314 50th Street, Suite 103, Lubbock, Texas 79412.

LEATHER

AVELLISYNCO



Selected Dyestuffs



 **CHEMTAN**

17 Noble Farm Drive • Lee, NH 03861 (Office)
57 Hampton Road • Exeter, NH 03833 (Manufacturing)
Tel: (603) 772-3741 • Fax: (603) 772-0796
www.CHEMTAN.com

Collagen Fiber Opening of Cattle Hides in Urea/Calcium Hydroxide Solutions

by

Qian Zhang,^{1,2†} Jie Liu,^{1†} Xiumin Li,¹ Hui Liu,¹ Yadi Hu¹ and Keyong Tang^{1*}

¹*School of Materials Science and Engineering, Zhengzhou University, Zhengzhou 450001, China*

²*High and New Technology Research Center of Henan Academy of Science, Zhengzhou 450001, China*

Abstract

In the beamhouse, liming might directly affect the structure and performance of collagen, as well as the quality of resultant leather. However, the influences of composition and content of liming agents on liming mechanism are quite complicated. In this study, calcium hydroxide and urea were utilized in liming. The solution pH, hide swelling ratio and non-collagenous protein removal were quantitatively analyzed. The morphologies of both limed and fresh hides were studied by optical microscopy. The reaction mechanism of fiber opening up of cattle hides was analyzed and speculated by the combination of thermogravimetric analysis and Fourier transformation infrared spectroscopy. It was found that the fiber bundles of hides limed by urea/calcium hydroxide have a better opening up effect than that by pure calcium hydroxide. The mechanism of liming in an urea/calcium hydroxide solution system was proposed.

Introduction

Animal hides are transformed into leathers through a series of leather making processes including soaking, fleshing, degreasing, unhairing, liming, deliming, bating, pickling and tanning.^{1, 2} Animal hides are mainly composed of three layers of grain surface/epidermis, dermis, and subcutaneous tissue. The dermis between the epidermis and subcutaneous tissue is the main component of leather. Leather making includes a lot of complicated processes affecting the structure of collagen, in which liming is one of the most critical steps that can determine the final style and properties of leather.³⁻⁸ It is widely accepted that after liming, the partial secondary bonds in collagen can be destroyed and some glycoproteins among the collagen fiber bundles are also removed. As a result, the collagen fiber bundles are opened to expose enough active sites for the penetration and reaction of subsequent leather chemicals.

Traditional liming is done in a complex aqueous system with lime, sulfide, alkaline, neutral salt, enzyme, liming auxiliaries and surfactant.⁹ However, most of these reagents cannot be fully utilized in the water medium, resulting in a waste of chemical reagents and environmental pollution.^{10,11} Marsal et al. studied the composition

and properties of wastewater from a tannery and proposed the recovery of nitrogen from wastewater in the beamhouse.¹² Mohamaed et al. studied the composition and change in liming wastewater.¹³ The recycling of liming wastewater was realized by adding chemicals to adjust its composition for 8 times of cycling. However, due to insufficient research on the contribution of each component to the liming and the interaction discipline among the components, it is still difficult to reveal the reaction process to reuse the liming agent.

With the increasing need for environmental protection, attention has been paid to greener and cleaner processes, such as biological treatments.¹⁴⁻¹⁹ For example, Ranjithkumar et al. used enzymes from solid-state fermentation for unhairing.²⁰ Leather samples unhaird by an enzymatic method showed better smoothness, finer grain pattern than those unhaird by conventional method. Sivasubramanian et al. used a bacterial protease based a commercial unhairing enzyme for enzyme-assisted unhairing.²¹ From the microscopic structure of goatskins, it was found that the hairs were not destroyed totally and the roots of the removed hairs were observed. Liu et al. developed a novel liming agent based on sodium silicate and enzyme to replace lime.²² The dosage of the liming agent was 1.5%, and the swelling ratio, fiber bundle opening, shrinkage temperature and mechanical properties of the leather were comparable to those of leather made by the conventional liming method.

In order to find a suitable liming condition to moderately disperse the collagen fibers, Liu et al. studied the effect of liming time on collagen fibers.²³ They determined the opening up degree of collagen fibers at different liming times by acoustic emission and found that the opening up degree of dermal collagen fibers was related to the liming time. Cheng et al. explored the changes of hides limed with alkali and neutral salts and found that a high concentration of sodium sulfate depressed the swelling of collagen fibers in alkali solutions, while no obvious effect was found in sodium chloride solution.²⁴ Tang et al. studied the changes in thermal degradation activation energy of collagen fibers and discussed the influence of alkali solution and urea solution treatment on the dry heat shrinkage properties.²⁵⁻²⁷

Currently, increasing effort has been focused on cleaner production in leather making. It is of great importance to know the liming

*Corresponding Author email: kytangzsu@hotmail.com

Manuscript received September 13, 2020, accepted for publication January 17, 2021.

†These authors contributed equally to this manuscript.

mechanism to find a more suitable liming system. In this work, the mechanism of liming in calcium hydroxide and urea/calcium hydroxide solutions was studied. In general, calcium hydroxide is a commonly used liming agent for collagen fiber bundle opening. The morphology of collagen fibers in different concentrations of calcium hydroxide was investigated using optical microscopy as well as scanning electron microscopy (SEM). The swelling ratio of cattle hides and the total protein, proteoglycan and hydroxyproline in wastewater were measured. Thermogravimetric (TG) and Fourier transformation infrared (FTIR) analyses were used to analyze the thermal properties and chemical structure of limed hides. Furthermore, as a good auxiliary agent for liming, urea was used instead of sodium sulfide for the purpose of reducing sulfide use and pollution.

Experimental

Materials

Wet-salted cattle hides were provided by Prosper Skins & Leather Enterprise Co., Ltd. (Jiaozuo, China). Sodium carbonate (Na_2CO_3), calcium hydroxide ($\text{Ca}(\text{OH})_2$), urea, ammonium sulfate ($(\text{NH}_4)_2\text{SO}_4$), and sulfuric acid were purchased from Civi Chemical Technology Co., Ltd. (Shanghai, China). Sodium chloride, tannic acid and dispase (50 U/mg) were from Macklin Biochemical Co., Ltd. (Shanghai, China).

Liming Treatment

Wet-salted cattle hides were used as raw materials and pre-treated by conventional leather making process before liming (Figure 1). After pre-treatment, the fresh hides were cut into small pieces sized

0.25 cm^2 for liming. Then the samples were stirred in two sets of liming solutions for 24 hours in beakers. The first set is pure calcium hydroxide solutions with the concentrations of 0.5 %, 2 %, 3.5 %, 5 % and 6.5 % (w/v), and the resulting samples limed by these solutions were named as P-0.5%Ca, P-2%Ca, P-3.5%Ca, P-5%Ca, and P-6.5%Ca, respectively. Another set is urea/calcium hydroxide solutions at weight ratios (urea:calcium hydroxide) of 1:2, 4:2, 7:2, 10:2, 13:2, and 16:2, and the samples limed by these solutions were coded as S-1%urea-2%Ca, S-4%urea-2%Ca, S-7%urea-2%Ca, S-10%urea-2%Ca, S-13%urea-2%Ca, and S-16%urea-2%Ca, respectively. After liming, the hides were delimed, bated, pickled and tanned with tannin acid. The procedure and detailed experimental conditions are illustrated in Figure 1.

pH of the Liming Solutions

The pH of the liming solutions was monitored with a PHS-3G pH meter (Shanghai Yidian Scientific Instrument Company, China) after the various liming times: 0 h, 1 h, 4 h, 8 h, 12 h and 24 h, respectively.

Swelling Ratios of Cattle Hides

Swelling ratios of the samples were calculated according to the following equation:²⁸

$$\Delta h\% = (h_i - h_0)/h_0 \times 100\% \quad (1)$$

where h_i is the thickness of the sample after liming for 24 h and h_0 is the thickness of the sample before liming. The thickness of hides was measured by a leather thickness gauge (Randall & Stickney Dial Company, USA). The thickness of leather samples was obtained after 1 min of compression at 50 kPa.

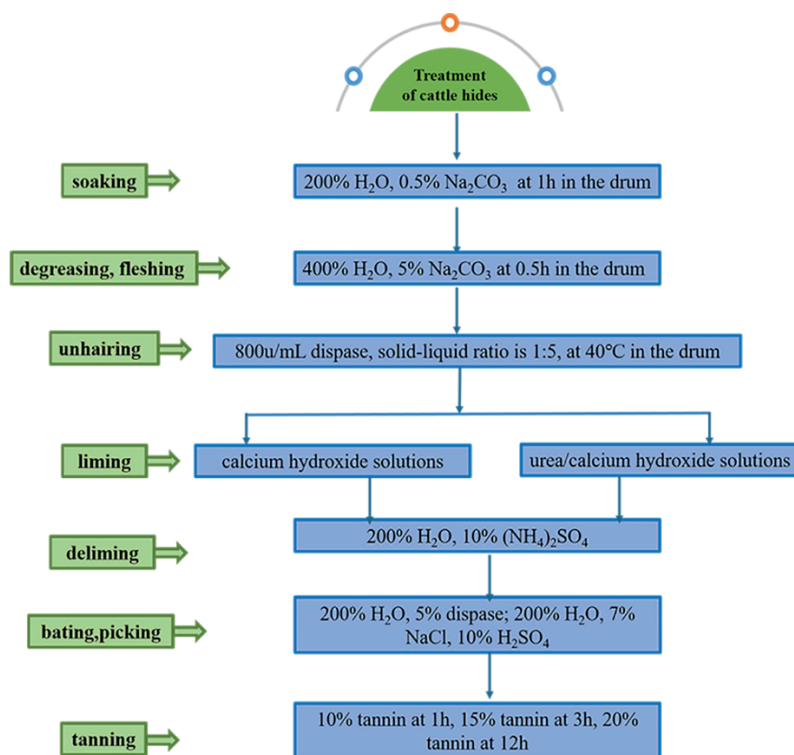


Figure 1. Schematic representation of the overall treatment of cattle hides.

Protein Content in Wastewater

The Bicinchoninic acid reagent was used to test the content of proteins in wastewater, whose mechanism is that Cu^{2+} can be reduced to Cu^+ by proteins under alkaline condition, and the complex formed by Cu^+ and bicinchoninic acid presents purple color with an absorption peak at 562 nm. Therefore, spectrophotometer (Thermo Fisher Scientific Oy Ratastie 2, FI-01620 Vantaa, Finland) was employed to characterize the absorbance of the complex at 562 nm, and the protein content in the wastewater was obtained by comparing the absorbance to the standard absorbance curve of protein at 562 nm.

Proteoglycan Content in Wastewater

In a boiling water bath, proteoglycan was dehydrated by sulfuric acid to form furfural or hydroxymethyl furfural and their derivatives through the dehydration condensation of anthrone ($\text{C}_{14}\text{H}_{10}\text{O}$). Furfural or hydroxymethyl furfural has a maximum absorption peak at 620 nm. Based on this principle, proteoglycan content was identified by adding sulfuric acid and anthrone reagents into the wastewater. The absorbance of furfural or hydroxymethyl furfural derivatives at 620 nm was recorded by an ultraviolet spectrophotometer (TU-1950, Beijing Purkinje General Instrument Co., Ltd., China). By comparing the absorbance of samples with the standard absorbance curve, the content of proteoglycan in the wastewater was calculated.

Hydroxyproline Content in Wastewater

Hydroxyproline was measured by Ehrlich methods according to the reported studies.^{29,30} Hydroxyproline may be oxidized by an oxidant (Chloramine T), and the oxidation products may react with dimethylaminobenzaldehyde to yield a purple color complex with an absorption peak at 550 nm. Similarly, the absorption peak of distilled water and hydroxyproline standard concentration at 550 nm was measured. The hydroxyproline content in the wastewater was obtained according to Eq. (2).

$$C_H = (OD_T - OD_C) / (OD_S - OD_C) \times C_S \times 10 \quad (2)$$

where C_H is the hydroxyproline content in the wastewater, OD_T is the absorbance of test sample in the wastewater, OD_C is the absorbance of control sample, OD_S is the absorbance of standard sample, and C_S is the content of standard sample of hydroxyproline.

Structure

After liming, samples of around 0.25 cm^2 were cut from the standard sampling area of the cattle hides. The samples were placed in paraformaldehyde solution for staining. The hide samples were subjected to Verhoeff's Van Gieson (EVG) staining for the observation of histological features using an optical microscope (Eclipse E100, Nikon, Japan). After tanning, the vegetable-tanned leather was freeze-dried in a GT2-Type-8 freeze dryer (LYOTECH, Germany). The samples of the vegetable-tanned leather were cut into thin strips. The strips were sprayed by a thin layer of gold under

vacuum conditions and observed by a Quanta 250 scanning electron microscopy (FEI, USA). The orientation of collagen fibers were observed from SEM for the cross-section at the accelerating voltage of 20 kV with different magnifications. After liming, the hides were delimed, washed and freeze-dried. The dried samples were analyzed by a TGA/DSC1 thermogravimetric analyzer (NETZSCH, Germany). Approximately 5~10 mg of samples were exposed to a nitrogen atmosphere at a flow rate of 140 mL/min, and heated in a ceramic sample pan at a heating rate of $10^\circ\text{C}/\text{min}$ from 25 to 600°C . The Fourier transform infrared (FTIR) spectra of hide samples were recorded using a VERTEX 70 spectrometer (Bruker Optik GmbH, Ettlingen, Germany). The spectrum was obtained ranging from 4000 cm^{-1} to 400 cm^{-1} at a resolution of 4 cm^{-1} , and the spectrum scan was conducted with 8-s intervals.

Results and Discussion

The pH of Liming Solutions

The pH is especially important in liming, which influences the swelling ratio of hides and even the properties of resultant leathers. Since the pH of the bath is higher than the isoelectric point of collagen, collagen molecules are negatively charged due to the dissociation of the carboxyl groups on the side chains, and collagen fiber bundles become shorter and thicker due to the electrostatic interactions with the adjacent protein chains and the hydration of the charged groups.³¹ This shows that the swelling of hides depends primarily on the difference between the bath pH and the isoelectric point of the collagen. Therefore, the pH of liming solutions was further studied in the present work and the results are shown in Figure 2. In Figure 2(a), the pH of calcium hydroxide solution is about 12.81, which changes slightly with the increase of calcium hydroxide concentration. It is also observed that the pH of calcium hydroxide solution is decreased after liming, illustrating that the liming agents dissolved in the water and penetrated into the hide. Figure 2(b) shows that the pH of the urea/calcium hydroxide solution increases from 12.83 to 13.01 with increasing the urea concentration, a little higher than that of the pure calcium hydroxide only. However, the pH of 1%~16% pure urea solutions is all about 7.4. Therefore, it was illustrated that urea might act as a solubilizer for calcium hydroxide in liming solution via coordination of Ca^{2+} with $\text{CO}(\text{NH}_2)_2$ in the urea/calcium hydroxide solutions.³²

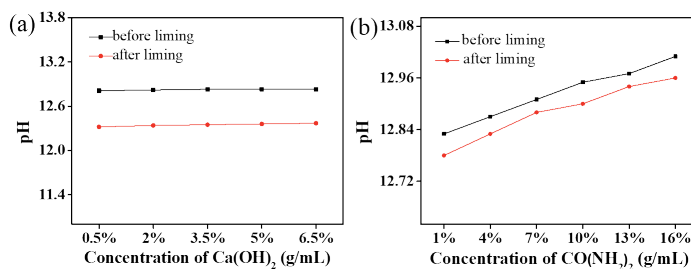


Figure 2. Variation of pH with the increase of (a) $\text{Ca}(\text{OH})_2$ concentration and (b) urea concentration with 2% $\text{Ca}(\text{OH})_2$.

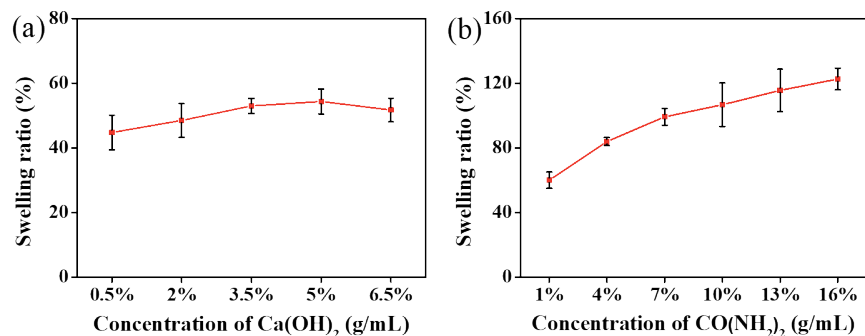


Figure 3. Variation of swelling ratio of hides with concentrations of (a) $\text{Ca}(\text{OH})_2$ and (b) urea (in the presence of 2% $\text{Ca}(\text{OH})_2$).

Swelling Ratio of Hides after Liming

Collagen fiber bundles become shorter and thicker as observed by optical microscopy, and a macroscopic swelling of hides can be observed after liming. Therefore, the swelling ratio of hides in liming was further studied. As shown in Figure 3(a), after liming, the swelling ratio of hides increases with increasing the calcium hydroxide concentration. Figure 3(b) shows that the swelling ratio of hides limed by urea/calcium hydroxide solution gradually increases with the increase of urea concentration. The hides limed by urea/calcium hydroxide solution showed a higher swelling ratio than those limed by a pure calcium hydroxide solution. The swelling ratio of hides limed by 2% $\text{Ca}(\text{OH})_2$ was 48.5 %, while those limed by urea/calcium hydroxide was in the range of 60.0~122.6%. Herein, the inter- or intra-molecular hydrogen bonding of collagen might be partially destroyed by urea, and then more water molecules might be able to enter into the hides to fully fill in the hides, resulting in a more obvious swelling.

Contents of Total Protein, Proteoglycan and Hydroxyproline in Wastewater

The contents of total protein, proteoglycan and hydroxyproline in liming wastewater might indicate the effect of liming on hides.³ The total protein and hydroxyproline content was determined by measuring the degree of collagen hydrolysis and the removal extent of non-collagenous protein content in the wastewater. The ability of liming agents to hydrolyze collagen fibers and dissolve the interstitial fibers is indirectly estimated by the content of proteins in the wastewater. As revealed in Table I, with the increase of calcium hydroxide concentration, the protein content in liming wastewater increases firstly and then decreases at a concentration higher than 3.5%. Here the protein may be coagulated with the precipitation of calcium hydroxide in the wastewater due to suspension of calcium hydroxide.³³ In addition, compared to that with the pure calcium hydroxide liming solution, the protein in the wastewater is increased by the addition of urea. Thus, more non-collagenous proteins of hides were removed in the urea/calcium hydroxide solution. The removal of proteoglycan aids in the collagen fiber bundle opening. The proteoglycan contents in liming wastewater are shown in Table I. The proteoglycan contents in urea/calcium hydroxide liming wastewater did not decrease obviously, compared to that limed in

pure calcium hydroxide solutions. Since hydroxyproline is a unique amino acid in collagen, the degree of collagen hydrolysis might be analyzed by the hydroxyproline contents in the wastewater.²⁸ As shown in Table I, the hydroxyproline content in the wastewater gradually increases with the calcium hydroxide concentration increasing. This reflects the fact that the degree of collagen hydrolysis increases with the calcium hydroxide concentration. However, the presence of urea in liming solution could restrict the hydrolysis of collagen, as manifested by the lower content of hydroxyproline in urea/calcium hydroxide liming wastewater when compared to those in pure calcium hydroxide liming wastewater. Therefore, it can be concluded that liming in urea/calcium hydroxide solution might be helpful for promoting collagen fiber bundles opening as well as keeping the integrity of collagen molecules.

Table I
Quantitative evaluation of beamhouse processes.

Samples	Total protein content ^a mg/mL	Proteoglycan content ^a μg/mL	Hydroxyproline content ^a μg/mL
P-0.5%Ca	0.21±0.01	199.8±7.1	1.35±0.06
P-2%Ca	0.22±0.04	225.0±15.4	2.90±0.06
P-3.5%Ca	0.23±0.05	288.6±40.4	3.27±0.09
P-5%Ca	0.17±0.01	135.7±15.2	3.54±0.07
P-6.5%Ca	0.17±0.00	163.3±11.1	3.91±0.08
S-1%urea-2%Ca	0.23±0.05	110.2±13.2	0.10±0.00
S-4%urea-2%Ca	0.24±0.01	214.2±13.2	0.26±0.02
S-7%urea-2%Ca	0.30±0.03	192.4±9.5	0.49±0.06
S-10%urea-2%Ca	0.26±0.03	279.9±18.2	0.84±0.03
S-13%urea-2%Ca	0.23±0.06	274.0±39.8	1.44±0.06
S-16%urea-2%Ca	0.20±0.03	313.6±45.4	1.25±0.04

^aAverage value of three test data.

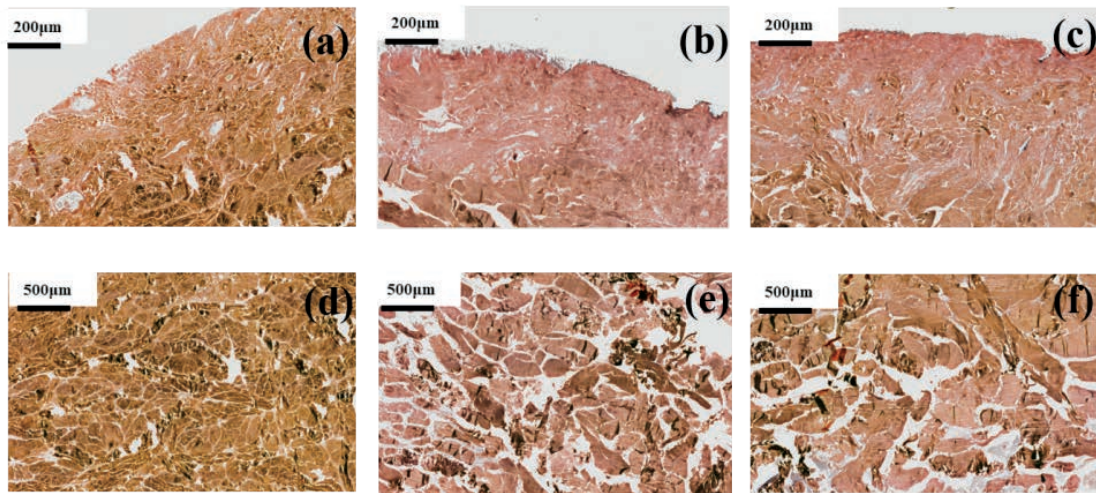


Figure 4. Histologically stained cross-section micrographs of (a, d) fresh hide, (b, e) P-2%Ca and (c, f) S-7%urea-2%Ca samples.

Histological Photographs and Scanning Electron Microscopy

In Figure 4, the constituents of the hair follicles and the tissues were stained as dark brown. The elastic fibers were stained as dark purple, and the collagen fibers were stained as dark red. Compared to the hides without liming, less non-collagenous proteins were revealed in hides limed by calcium hydroxide and urea/calcium hydroxide solutions, indicating more opening up of collagen fibers by liming. The cross-sectional SEM micrographs of vegetable-tanned leathers are shown in Figure 5. It can be observed that the vegetable-tanned leather limed by 7%urea/2%Ca(OH)₂ solution

(Figure 5(c,d)) shows better collagen fiber bundle opening than that of limed in 2% Ca(OH)₂ solution (Figure 5(a,b)). These results are consistent with the above-discussed protein contents in liming wastewater (Table I).

TG Results

The thermogravimetric (TG) and differential thermogravimetric (DTG) curves of various limed hides are given in Figure 6. Similar curves were found for all the samples. The evaporation temperature of unbound water is around 100°C. The thermal decomposition

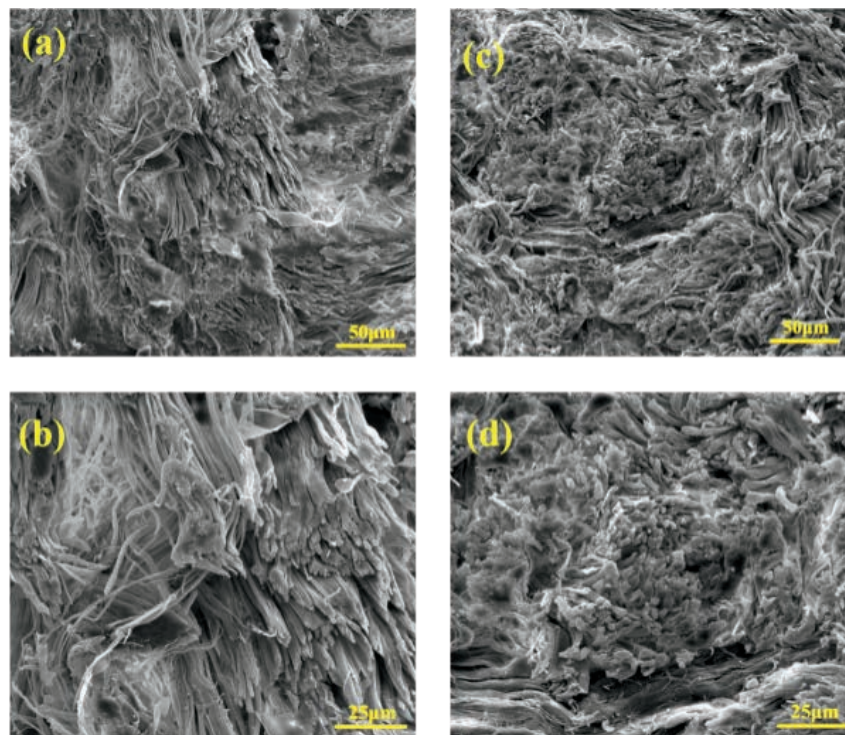


Figure 5. SEM micrographs of the cross-section of vegetable-tanned leather limed in (a, b) 2% Ca(OH)₂ and (c, d) 7% urea/2% Ca(OH)₂ solutions.

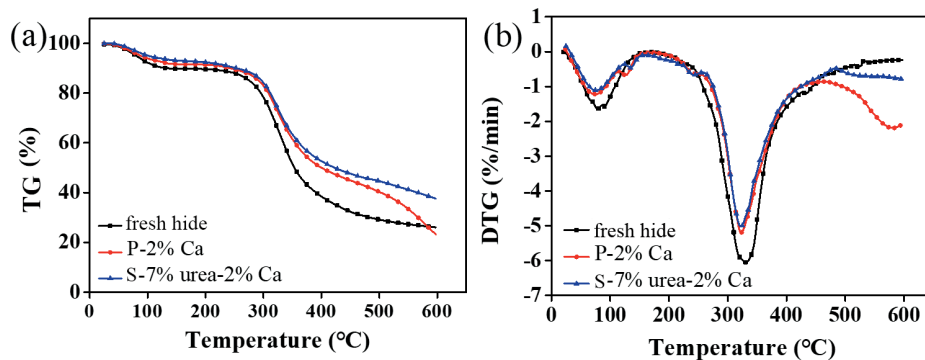


Figure 6. (a) TG and (b) DTG curves of hides limed by different liming systems.

temperature of collagen begins at around 200°C and is completed at around 450°C in both hides before limed and limed with urea/ $\text{Ca}(\text{OH})_2$.^{34,35} Table II shows the onset temperature and weight loss percentage at 600°C. The onset temperature of hides limed by 7% urea/2% $\text{Ca}(\text{OH})_2$ is higher than that of the fresh hide, suggesting a better thermal stability of hides limed by 7% urea/2% $\text{Ca}(\text{OH})_2$

Table II

The onset temperature and weight loss ratio of hides limed with different liming systems.

Samples	Onset temperature (°C)	Weight loss percentage at 600°C (%)
Fresh hide	288.8	74.0
P-2%Ca	286.1	77.3
S-7%urea-2%Ca	292.7	62.4

solution than the fresh hide. However, the onset temperature of hides limed by 2% $\text{Ca}(\text{OH})_2$ solution is lower than the fresh hide, indicating that liming by calcium hydroxide decreases the thermal stability of hides. Interestingly, the weight loss percentage of hides limed by 2% $\text{Ca}(\text{OH})_2$ is more than that of fresh hide, while that of hides limed by 7% urea/2% $\text{Ca}(\text{OH})_2$ solution is the lowest of the three samples.

Possible Liming Mechanism

According to the results discussed above, the possible liming mechanism in different liming solutions can be proposed. In pure $\text{Ca}(\text{OH})_2$ solution, the hydrogen bonding in collagen may be disrupted by the hydroxyl ions in calcium hydroxide solution, and some Ca^{2+} may combine with carboxyl groups in collagen by cooperation interactions (Figure 7(A)). Urea is a well-known hydrogen-bond-breaking reagent. The schematic illustration of the disruption of the hydrogen bonds in collagen matrix by urea is shown in Figure 7(B). Moreover, both the pH of urea/ $\text{Ca}(\text{OH})_2$

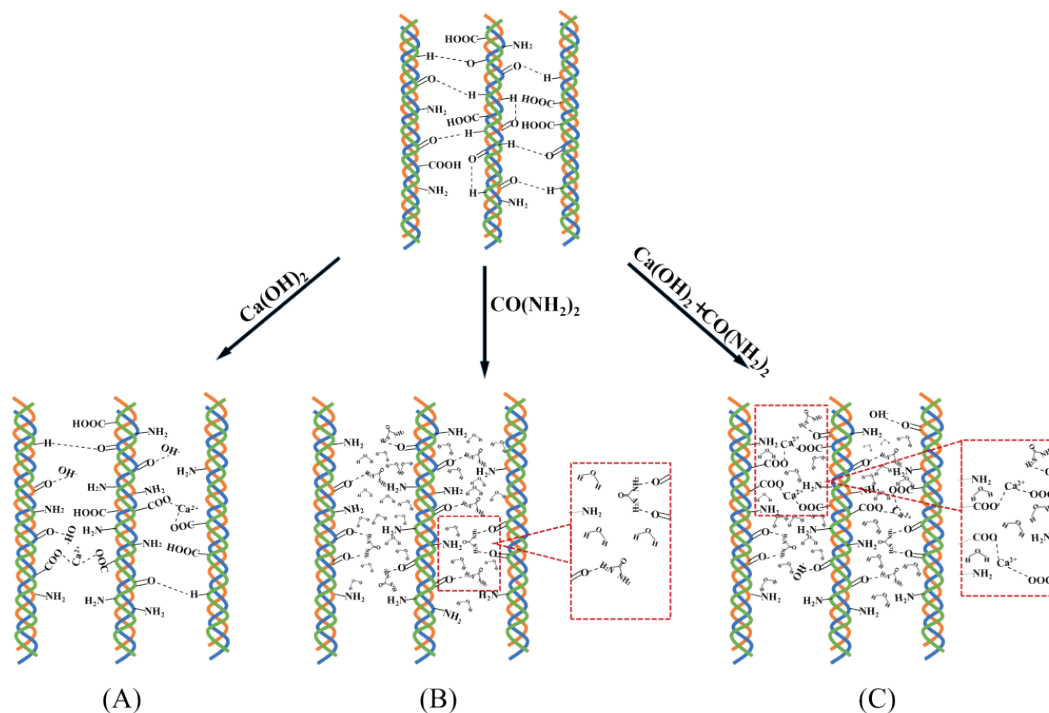


Figure 7. The mechanism of liming in (A) calcium hydroxide and (C) urea/calcium hydroxide solution; (B) The disrupting mechanism of hydrogen bonding in collagen matrix by urea.

solution (Figure 2) and swelling ratio of hides limed by urea/ $\text{Ca}(\text{OH})_2$ (Figure 3) are higher than those of the samples limed only by $\text{Ca}(\text{OH})_2$. Based on these facts, it can be speculated that the inter- and intra-molecular hydrogen bonding of collagen molecules may be disrupted by urea and calcium hydroxide synergistically, and thereby exposing more sites on the collagen to lime. To be specific, hydrogen bonding in collagen may be disrupted collaboratively by the amino groups (from $\text{CO}(\text{NH}_2)_2$) and hydroxyl ions (from $\text{Ca}(\text{OH})_2$) in urea/ $\text{Ca}(\text{OH})_2$ solution. Consequently, the Ca^{2+} in the solution may combine with more carboxyl groups on collagen by coordination, resulting in a higher thermal stability of hides limed by urea/ $\text{Ca}(\text{OH})_2$ than that of other two samples (Figure 7(C)). The changes in thermal stability of the hides can be seen from Table II, and the weight loss at 600°C of the hide limed by urea/ $\text{Ca}(\text{OH})_2$ is the lowest among the three samples. This may be attributed to the formation of more coordination compounds within the collagen matrix after liming with urea/ $\text{Ca}(\text{OH})_2$ solution.

In this work, the complexation mechanism of Ca^{2+} and carboxyl groups in collagen was investigated by FTIR spectra in the range of $500\text{--}4000\text{ cm}^{-1}$. The FTIR spectra of hides (Figure 8) revealed the typical characteristic peaks of collagen.³⁶⁻³⁸ The absorbance bands of the amide A of collagen are located at 3304 cm^{-1} , mainly due to the stretching vibration absorption peak of N-H and O-H. The band near 3078 cm^{-1} responds to the amide B of collagen, which should be assigned to the asymmetric and symmetric stretching vibration absorption peak of $-\text{CH}_2$. Besides, the characteristic absorbance bands of amide I, amide II and amide III modes of collagen were all observed at 1633 cm^{-1} , 1540 cm^{-1} and 1235 cm^{-1} , respectively. Formation of amide I is mainly by stretching vibration absorption peak of C=O. Especially, the vibration peak of C=O at 1750 cm^{-1} indicated the existence of carboxyl group. Compared with that of the fresh hide, the peak intensity of amide A, amide I and C=O of the hides limed with $\text{Ca}(\text{OH})_2$ and urea/ $\text{Ca}(\text{OH})_2$ is weakened, indicating that the amount of carboxyl group is reduced by liming. Hence, the carboxyl group of collagen may react with Ca^{2+} by coordination.

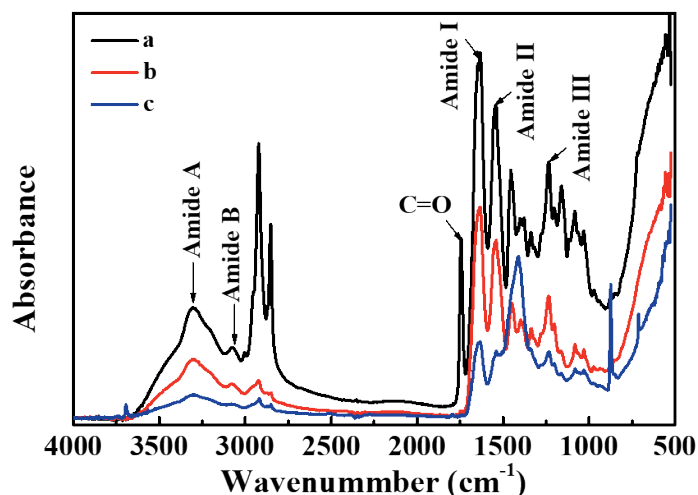


Figure 8. FTIR spectra of (a) fresh hide, (b) P-2%Ca, (c) S-7%urea-2%Ca.

Conclusions

In this study, the effect of urea/calcium hydroxide on the collagen fiber bundles in liming is studied by histological and SEM analyses. The results indicated that the 7% urea/2% $\text{Ca}(\text{OH})_2$ solution is the best for liming from viewpoints of collagen fiber bundle opening. Urea/calcium hydroxide has greater ability to remove the interfibrillar substance, compared with that of pure calcium hydroxide. The combination of urea with calcium hydroxide has a good opening up effect for collagen fiber bundles. A possible mechanism of liming in calcium hydroxide and urea/calcium hydroxide solution system was proposed based on the results obtained. The inter- and intra-molecular hydrogen bonding of collagen molecules may be destroyed by urea, making the penetration of molecular water into the collagen networks easier.

Acknowledgements

The financial supports from the National Key R & D Program of China (No. 2017YFB0308500), National Natural Science Foundation Commission of China (No. 51673177) and the Key Scientific Research Projects of Henan Province (No. 21A430034) are greatly appreciated.

References

1. Wu, J., Zhao, L., Liu, X., Chen, W. and Gu, H.; Recent progress in cleaner preservation of hides and skins. *Journal of Cleaner Production* **148**, 158-173, 2017.
2. Zhang, Y., Liu, H., Wang, F. and Tang, K.; KCl-assisted enzyme in unhairing and collagen fibre bundle opening for cleaner leather making. *Journal of the Society of Leather Technologists and Chemists* **104**(5), 235-239, 2020.
3. Li, S., Li, J., Yi, J. and Shan, Z.; Cleaner beam house processes trial on cattle sofa leather. *Journal of Cleaner Production* **18**(5), 471-477, 2010.
4. Tang, K., Li, W., Liu, J., Liu, C.-K. and Pan, H.; Mechanism of collagen processed with urea determined by thermal degradation analysis. *JALCA* 2020, **115**(10): 380-389, 2020.
5. Liu, H., Li, X., Li, M., Zhang, Y., Tang, K., Liu, J., Zheng, X. and Pei Y.; A simple and sustainable beamhouse by the recycling of wastewater from KCl-dispase synergistic unhairing in leather making. *Journal of Cleaner Production* **282**, 124535, 2020.
6. Saravanan, P., Renitha, T. S., Gowthaman, M. and Kamini, N.; Understanding the chemical free enzyme based cleaner unhairing process in leather manufacturing. *Journal of Cleaner Production* **79**, 258-264, 2014.
7. Kanagaraj, J., Senthilvelan, T., Panda, R. C. and Kavitha, S.; Eco-friendly waste management strategies for greener environment towards sustainable development in leather industry: A comprehensive review. *Journal of Cleaner Production* **89**, 1-17, 2015.
8. Kanagaraj, J., Panda, R., Senthilvelan, T. and Gupta, S.; Cleaner approach in leather dyeing using graft copolymer as high

- performance auxiliary: related kinetics and mechanism. *Journal of Cleaner Production* **112**, 4863-4878, 2016.
9. Liu, H., Yin, Z., Zhang, Q., Li, X., Tang, K., Liu, J., Pei, Y., Zheng, X. and Ferah, C. E.; Mathematical modeling of bovine hides swelling behavior by response surface methodology for minimization of sulfide pollution in leather manufacture. *Journal of Cleaner Production* **237**, 117800, 2019.
 10. Sathish, M., Madhan, B., Sreeram, K. J., Rao, J. R. and Nair, B. U.; Alternative carrier medium for sustainable leather manufacturing-A review and perspective. *Journal of Cleaner Production* **112**, 49-58, 2015.
 11. Yan, T., Luo, X., Zou, Z., Lin, X. and Yu, H.; Adsorption of Uranium(VI) from a simulated saline solution by alkali-activated leather waste. *Industrial and Engineering Chemistry Research* **56**, 3251-3258, 2017.
 12. Marsal, A., Bautista, E., Cuadros, S., Reyes, M., Rius, A. and Font, J.; Recovery of organic nitrogen from beamhouse wastewater in a hair recovery process. *Journal of the Society of Leather Technologists and Chemists* **93**, 176-182, 2009.
 13. Mohamaed, K. E. A. and Gasmelseed, G. A.; Recycling of unhairing lime liquors. *Journal of the Society of Leather Technologists and Chemists* **87**, 116-118, 2003.
 14. Shi, B., Lu, X. and Sun, D.; Further investigations of oxidative unhairing using hydrogen peroxide. *JALCA* **98**, 185-192, 2003.
 15. Valeika, V., Beleska, K., Valeikienė, V. and Kolodzeiskis, V.; An approach to cleaner production: from hair burning to hair saving using a lime-free unhairing system. *Journal of Cleaner Production* **17**, 214-221, 2009.
 16. Cheng, J., Yue, C., Jiang, S., Gao, Y., Nie, J. and Fang, S.; Synthesis and performances of UV-curable polysiloxane-polyether block polyurethane acrylates for PVC leather finishing agents. *Industrial and Engineering Chemistry Research* **54**, 5635-5642, 2015.
 17. Yi, Z., Ingham, B., Cheong, S., Ariotti, N. and Prabakar, S.; Real-time synchrotron small-angle X-ray scattering studies of collagen structure during leather processing. *Industrial and Engineering Chemistry Research* **57**, 63-69, 2017.
 18. Madhan, B., Rao, J. R. and Nair, B. U.; Studies on the removal of inter-fibrillary materials. I. Removal of protein, proteoglycan, glycosaminoglycans from conventional beamhouse process. *JALCA* **105**, 145-149, 2010.
 19. Dettmer, A., Cavalli, É., Ayub, M. A. Z. and Gutterres, M.; Optimization of the unhairing leather processing with enzymes and the evaluation of inter-fibrillary proteins removal: an environment-friendly alternative. *Bioprocess and Biosystems Engineering* **35**, 1317-1324, 2012.
 20. Ranjithkumar, A., Durga, J., Ramesh, R., Rose, C. and Muralidharan, C.; Cleaner processing: a sulphide-free approach for depilation of skins. *Environmental Science and Pollution Research* **24**, 1-9, 2017.
 21. Sivasubramanian, S., Manohar, B. M., Rajaram, A. and Puvanakrishnan, R.; Ecofriendly lime and sulfide free enzymatic dehairing of skins and hides using a bacterial alkaline protease. *Chemosphere* **70**(6), 1015-1024, 2008.
 22. Liu, Y., Chen, Y., Fan, H., Hu, Z., Luo, Z. and Shi, B.; Environment-friendly lime-free liming. *Journal of the Society of Leather Technologists and Chemists* **93**, 56-60, 2009.
 23. Liu, C.-K., Latona, N. and Dimaio, G. L.; Degree of opening up of the leather structure characterized by acoustic emission. *JALCA* **96**, 367-381, 2001.
 24. Cheng, H., Chen, M. and Li, Z.; Properties of collagen fibre in alkali and neutral salt solutions. *Journal of the Society of Leather Technologists and Chemists* **94**, 65-69, 2010.
 25. Tang, K., Wang, F., Jia, P., Liu, J. and Wang, Q.; Thermal degradation kinetics of sweat soaked cattlehide collagen fibers. *JALCA* **102**, 52-61, 2007.
 26. Hu, Y., Liu, J., Luo L., Li X., Wang F. and Tang, K.; Kinetics and mechanism of thermal degradation of aldehyde tanned leather. *Thermochimica Acta* **691**, 178717, 2020.
 27. Tang, K., Liu, J., Wang, F., Liu, J. and Zhang, J.; Influence of urea process on thermal degradation behavior of collagen fibers. *China Leather* **33**, 25-27, 2004.
 28. Ding, Z. and Zhang, M.; Linear relationship between collagen degradation and degree of swelling in the beamhouse. *Journal of the Society of Leather Technologists and Chemists* **85**, 164-166, 2001.
 29. Bergman, I. and Loxley, R.; Two improved and simplified methods for the spectrophotometric determination of hydroxyproline. *Analytical Chemistry* **35**, 1961-1965, 1963.
 30. Stegemann, H. and Stalder, K.; Determination of hydroxyproline. *Clinica Chimica Acta* **18**, 267-273, 1967.
 31. Winkler, R.; On the existence of a lyotropic and osmotic type of collagen swelling produced by representative electrolytes and anelectrolytes. *Pflugers Archiv-european Journal of Physiology* **345**, 37-42, 1973.
 32. Fast, J., Hakansson, M., Muranyi, A., Gippert, G. P., Thulin, E., Evenas, J., Svensson, L. A. and Linse, S.; Symmetrical stabilization of bound Ca²⁺ ions in a cooperative pair of EF-hands through hydrogen bonding of coordinating water molecules in calbindin D9k. *Biochemistry* **40**, 9887-9895, 2001.
 33. Dickinson, E.; Milk protein interfacial layers and the relationship to emulsion stability and rheology. *Colloid Surface B* **20**, 197-210, 2001.
 34. Luo, L., Liu, J., Liu, C.-K., Brown, E. M., Wang, F., Hu, Y. and Tang, K.; Thermogravimetric analysis and pyrolysis kinetics of tannery wastes in an inert atmosphere. *JALCA* **115**, 123-131, 2020.
 35. Liu, J., Luo, L., Zhang, Z., Hu, Y., Wang, F., Li, X. and Tang, K.; A combined kinetic study on the pyrolysis of chrome shavings by thermogravimetry. *Carbon Resources Conversion* **3**, 156-163, 2020.
 36. Meng, Z., Zheng, X., Tang, K., Liu, J., Ma, Z. and Zhao, Q.; Dissolution and regeneration of collagen fibers using ionic liquid. *International Journal of Biological Macromolecules* **51**(4), 440-448, 2012.
 37. Lazarev, Y. A., Grishkovsky, B. and Khromova, T.; Amide I band of IR spectrum and structure of collagen and related polypeptides. *Biopolymers* **24**, 1449-1478, 1985.
 38. Liu, C.-K., Latona, N. P., Taylor, M. and Aldema-Ramos, M. L.; Biobased films prepared from collagen solutions derived from un-tanned hides. *JALCA* **110**, 25-32, 2015.

Oxidized Maltodextrin: A Novel Ligand for Aluminum–Zirconium Complex Tanning

by

Xueru Guo,¹ Yue Yu,^{1,1*} Ya-nan Wang^{1,2,**} and Bi Shi^{1,2}

¹National Engineering Research Center of Clean Technology in Leather Industry,
Sichuan University, Chengdu 610065, China

²Key Laboratory of Leather Chemistry and Engineering of Ministry of Education,
Sichuan University, Chengdu 610065, China

Abstract

Hydrogen peroxide (H₂O₂) oxidized maltodextrin was prepared as the ligand for aluminum–zirconium complex tanning. The effects of catalyst dosage, initiation temperature, and H₂O₂ dosage on maltodextrin oxidation were investigated. FT-IR analysis demonstrated that carboxyl groups were successfully introduced into oxidized maltodextrin. The carboxyl content and degradation degree of oxidized maltodextrin increased with the increase of H₂O₂ dosage. Maltodextrin oxidized by 40% H₂O₂ and 0.015% Cu–Fe catalyst at an initiation temperature of 70°C (OD-40) with moderate carboxyl group (6.75 mmol/g) and molecular weight (*M_w* 450) promoted the penetration and fixation of aluminum–zirconium salts in leather and showed better tanning performance, such as hydrothermal stability and porosity of leather, than traditional citric acid ligand.

Introduction

Developing effective chrome-free tannages to eliminate chrome discharge from the source is one of the key tasks of sustainable development of leather industry.^{1–4} Aluminum and zirconium salts have been regarded as alternatives to chrome tanning agent for a long time due to their similar tanning effects with chrome salts.^{5–7} However, aluminum and zirconium salts possess relatively high hydrolysis and olation ability,⁸ thereby resulting in their fixation on leather surface and uneven distribution through the cross-section. As a result, leather tanned with aluminum/zirconium salts commonly shows unsatisfactory physical and organoleptic properties such as rough and stiff handle.

There are two possible ways to solve the problem. The first one is to combine aluminum and zirconium salts together and form a heteronuclear complex tanning agent.⁹ The second one is to introduce ligands (masking agents for tanning) into the complexes.¹⁰ These modifications aim to slow down the reactivity and raise the alkali resistant ability of Al(III)/Zr(IV). Thus, hydrolysis and olation of aluminum/zirconium salts will be inhibited to some extent and

tanning performance is expected to be improved.⁸ Some hydroxy carboxylic acids, such as lactic acid, citric acid, malic acid and tartaric acid, were reported as ligands of aluminum/zirconium complexes before.^{9,10} However, limited enhancement to the tanning performance was achieved and few practical examples of industrial scale were performed. This result should be attributed to the inappropriate coordination ability and molecular size of the present ligands. Therefore, it is necessary to seek new ligands and clarify their structure-property relations in the development of metal complex tanning.

Our previous work reported a type of highly-oxidized starch (HOS) prepared using H₂O₂ and its application as ligand for zirconium and aluminum-zirconium complex tanning.^{11–14} The multiple hydroxyl groups on the anhydroglucose unit of starch were oxidized into carboxyl groups by H₂O₂, accompanied by the degradation of starch. An optimized HOS ligand with proper carboxyl content and molecular weight was obtained through regulating oxidation degree and the complex tanning performance was proven to be upgraded when HOS was introduced into the tanning system. The major difficulty of this technology occurred in the preparation of HOS. Starch, as a natural polymer, was in high viscosity and low concentration when dissolved in water,¹⁵ thereby leading to severe oxidation conditions and high dosage of H₂O₂ during production. In addition, the product quality was hard to control.

Maltodextrin, produced from starch by enzymatic hydrolysis, exhibits lower molecular weight and higher solubility than starch,¹⁶ which may favor the control of the oxidation reaction and industrial production of high-solid-content ligand. In this study, oxidized maltodextrin ligand using H₂O₂ was prepared under relatively mild oxidation conditions. Effects of catalyst dosage, initiation temperature and H₂O₂ dosage on maltodextrin oxidation were investigated. The relationship between the structure of oxidized product and the tanning performance of aluminum–zirconium–oxidized maltodextrin complexes was explored. We hope this work will provide a promising and practical chrome-free tanning for sustainable development of leather industry.

Experimental

Materials

Maltodextrin (DE value of 19) and hydrogen peroxide (50 wt%) were of commercial grade and provided by a leather chemical company. Pickled cow hides were supplied by a tannery in Jiangsu Province, China. Amberlite IR120 strong-acid cation exchange resin was purchased from Sigma-Aldrich LLC. The other chemicals used for analysis were of analytical grade. The chemicals used for leather processing were of industrial grade.

Preparation of Oxidized Maltodextrin

Four hundred grams of maltodextrin was dissolved in 267 g water. Different amounts (0.005%, 0.010%, 0.015% and 0.025%, based on the weight of maltodextrin, the same below) of catalyst ($\text{CuSO}_4 \cdot 5\text{H}_2\text{O}$ and $\text{FeSO}_4 \cdot 7\text{H}_2\text{O}$ in a mass ratio of 2:8) were introduced, and then a certain amount of H_2O_2 (20%, 30%, 40%, 50% and 60%, respectively) was dropwise added under stirring at different temperatures (60, 70, 80 and 90°C). After the addition of H_2O_2 , the oxidation proceeded at 90°C for another 1 h to obtain the product. During this period, samples were collected at 0, 15, 30, 45 and 60 min for measuring decomposition rate of H_2O_2 , carboxyl content and colority. The products oxidized by different amounts of H_2O_2 were marked as OD-20 (oxidized by 20% H_2O_2 , similarly hereinafter), OD-30, OD-40, OD-50 and OD-60.

Determination of Decomposition Rate of H_2O_2

Iodometric titration method was used for determining the decomposition rate of H_2O_2 .¹¹ In brief, oxidized maltodextrin samples were mixed with sulfuric acid, potassium iodide and ammonium molybdate, kept in a dark place for 10 min, and then titrated with sodium thiosulfate. Maltodextrin solution was used for the blank titration. The concentration of H_2O_2 in the samples was calculated. Decomposition rate of H_2O_2 was then calculated by the initial and the final H_2O_2 concentrations of the reactant/product.

Determination of Carboxyl Content

Acid-alkali titration method was used for determining the carboxyl content of oxidized maltodextrin samples.¹¹ In brief, the sample was loaded on a column (3.0 cm × 75 cm) filled with strong-acid cation exchange resin, and then eluted with ultrapure water. The eluate was titrated with sodium hydroxide using phenolphthalein as indicator. Maltodextrin solution was used for the blank titration. The carboxyl content of sample was calculated.

Determination of Colority

Platinum-cobalt colorimetric method was used for determining the colority of oxidized maltodextrin samples.¹⁷ The sample solution was diluted 25 times with ultrapure water, and then the colority of diluent was measured by a Pt-Co colorimeter (EC 2000, Loviband, UK). Ultrapure water was used for the background correction.

Fourier Transform Infrared (FT-IR) Spectroscopy Analysis

The FT-IR spectra of maltodextrin and oxidized maltodextrin samples were obtained using a FT-IR spectrometer (Nicolet 6700, Thermo Scientific, USA). Oxidized maltodextrin samples were lyophilized using a freezer dryer (LGJ-30F, Xinyi, China). The mixture of sample and potassium bromide was pressed into a thin disk before analysis.

Determination of Molecular Weight and Particle Size

The weight-average molecular weight (M_w) of maltodextrin and oxidized maltodextrin samples were measured by gel permeation chromatography (Viscotek 270maxGPC, Malvern, UK).¹¹ The sample solution with a mass concentration of 10 mg/mL was filtered through a 0.25 μm microporous membrane. Then, 100 μL filtrate was injected into a column (7.8 cm × 30 cm, TSK-gel GMPWXL, Tosoh, Japan) and eluted by 0.1 mol/L NaNO_3 at a flow rate of 0.6 mL/min under 40°C. The Shodex pullulan standard P-5 (2 mg/mL, M_w 6.1 × 10³, Showa Denko K.K., Japan) was used for reference. The calculation of molecular weight of the sample was performed using OmniSEC 4.7 software with a dn/dc value of 0.146 mL/g. The particle size of samples (200 mg/mL) was determined using a particle size analyzer (Nano Brook Omni, Brookhaven, US) with a test temperature of 30°C and an equilibration time of 3 min.

Tanning Trials

One pickled cattle hide was cut along the back bone into matching pieces (50 cm × 40 cm) for the tanning trials. They were weighed and tanned with aluminum–zirconium salts (70 wt% $\text{Al}_2(\text{SO}_4)_3 \cdot 18\text{H}_2\text{O}$ and 30 wt% $\text{Zr}(\text{SO}_4)_2 \cdot 4\text{H}_2\text{O}$) and different ligands (OD-20, OD-30, OD-40, OD-50, and OD-60) as shown in Table I. A group without any ligand was used as control. Another group with citric acid (CA) ligand was performed for comparison. All groups were named after the name of the ligands, except for the control. The shrinkage temperature (T_s) of the wet white was measured using a shrinkage temperature tester (MSW-YD4, Sunshine Electronic Research Institute, China). The wet white was split into three uniform layers and dried to constant weight at 102°C. Metal oxide content (the sum of Al_2O_3 and ZrO_2 , based on the weight of dry leather) of each layer and the whole leather were determined using ICP-OES (Optima 8000, PerkinElmer, USA). The metal oxide content in grain layer was named as *G*, in middle layer was named as *M*, and in flesh layer was named as *F*. The distribution uniformity of tanning agent was calculated as:¹²

$$\text{Distribution uniformity (\%)} = \frac{2 \times M}{G + F} \times 100$$

The wet white was lyophilized using a freezer dryer, and its cross-section was observed using SEM (JSM-7500F, JEOL, Japan). The porosity of the wet white was measured by mercury intrusion porosimetry using AutoPore IV 9500 analyzer (Micromeritics, USA).¹⁸

Table I
Al–Zr complex tanning process for cattle hide

Process	Chemicals	Dosage ^a (%)	Temperature (°C)	Time (min)	Remarks
Tanning	Water	80	25	30	
	Sodium chloride	5.6			
	Aluminum–zirconium salts	8.5	240		
	Ligand	1.2			
Basification	Magnesium oxide	1.2	40	100	pH 4.0 Overnight
	Sodium bicarbonate	0.2 × n		15 × n	
	Water	200		120	

Next day run for 30 min and drain → Horse up for 24 h

^aThe percentage of chemicals in Al–Zr complex tanning was based on limed pelt weight.

Table II
Post-tanning process

Process	Chemicals	Dosage ^a (%)	Temperature (°C)	Time (min)	Remarks	
Rewetting	Water	400	35	40		
	Degreasing agent	0.5				
	Water	400 × 2				10 × 2
Neutralizing	Water	200	35	30	pH 6.0	
	Neutralizing syntan	2				
	Sodium formate	1				
	Sodium bicarbonate	0.6 × 2				15 + 60
	Water	400 × 2				10 × 2
Fatliquoring	Water	150	50	60	pH 3.8	
	Synthetic fatliquor	15				
	Formic acid	0.5 × 4				15 × 4
	Water	200				25

Horse up overnight → Hang drying → Conditioning → Milling

^aThe percentage of chemicals in post-tanning was based on shaved wet white weight.

The wet white was wrung and shaved to uniform thickness (1 mm), and then post-tanning was performed as shown in Table II to obtain the crust leather. The crust leathers were conditioned for 48 h at 20°C and 65% RH, and then their physical properties, such as softness, tensile strength, tear strength, and bursting strength were measured.

Results and Discussion

Effect of Catalyst Dosage on Maltodextrin Oxidation

The hydroxyl groups on maltodextrin were oxidized into carboxyl groups by H₂O₂. Salts of Cu–Fe can be used as catalysts in the oxidation.¹² Figure 1 shows the effect of catalyst dosage on maltodextrin oxidation. The oxidation reaction was not conducted

efficiently without catalyst, as the decomposition rate of H₂O₂ and carboxyl content of oxidized maltodextrin were both low. The decomposition rate of H₂O₂ was enhanced with the increase of catalyst dosage, thereby resulting in the increase of carboxyl content of oxidized maltodextrin. When the amount of catalyst was 0.015%, H₂O₂ was exhausted in 15–30 min, and the carboxyl content stabilized at around 6.4 mmol/g. Further addition of catalyst dosage and reaction time did not improve the oxidation degree. Thus, the catalyst dosage was set to be 0.015%. It should be noted that the color of product became dark brown gradually once H₂O₂ was exhausted (see colority in Figure 1c), which may give leather unexpected color during tanning. This phenomenon can be explained by the dehydration reaction of sugar and formation of colored substances.^{19,20}

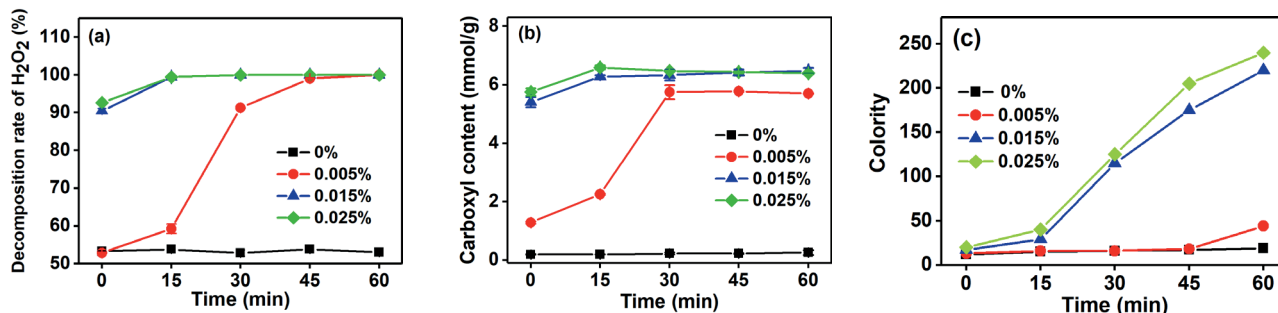


Figure 1. Effects of catalyst dosage on decomposition rate of H₂O₂ (a), carboxyl content (b) and colority (c) of oxidized maltodextrin (H₂O₂ dosage 40%, initiation temperature 70°C).

Effect of Initiation Temperature on Maltodextrin Oxidation

Oxidation by H₂O₂ under acidic condition follows a free-radical mechanism in presence of Cu–Fe salts. The formation of hydroxyl free radicals may be influenced by the initiation temperature. Figure 2 shows the effect of initiation temperature on maltodextrin oxidation. The decomposition of H₂O₂ was almost complete when the initiation temperature ranged from 60 to 90°C. The carboxyl content (representing oxidation degree) reached a peak at the initiation temperature of 70°C. Further raising the initiation temperature resulted in a slight decline of the carboxyl content. This result may be attributed to the higher risk of ineffective decomposition of H₂O₂ into water and oxygen under higher temperature.²¹ The colority of product showed a small growth with the increase of initiation temperature. Thus, the initiation temperature was set to be 70°C in consideration of oxidation degree and energy consumption.

Effect of H₂O₂ Dosage on Maltodextrin Oxidation

The effect of H₂O₂ dosage on maltodextrin oxidation is shown in Figure 3. In 30 min H₂O₂ was almost exhausted for each group, and the carboxyl content of oxidized maltodextrin formed a plateau from this point on. Then the colority of product rose sharply. The carboxyl content of product had a positive correlation with the H₂O₂ dosage, indicating a gradual growth of oxidation degree with the increase of H₂O₂ addition.

FT-IR spectra (Figure 4) also show that a new peak at 1733 cm⁻¹ is found in each of the oxidized maltodextrin compared with the spectrum of maltodextrin. This peak is assigned to the stretching vibration of carbonyl groups,²² demonstrating that carboxyl groups were introduced into oxidized product. The intensity of the peak is enhanced with the increase of H₂O₂ dosage, which is in accordance with the carboxyl content shown in Figure 3b. Moreover, Peaks

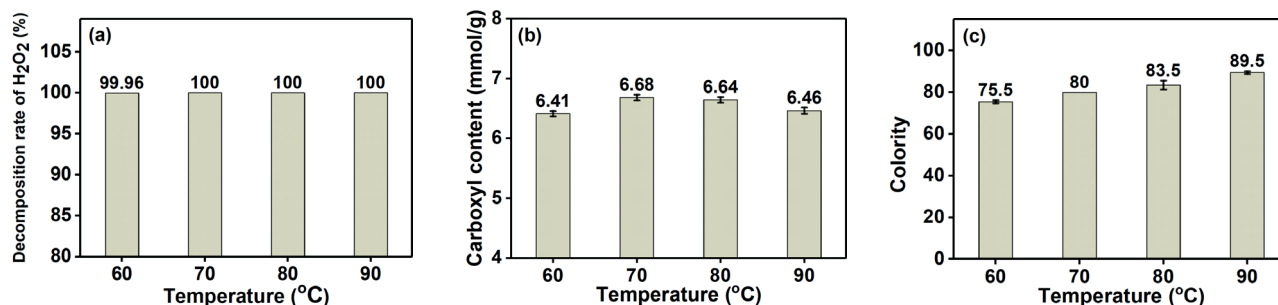


Figure 2. Effects of initiation temperature on decomposition rate of H₂O₂ (a), carboxyl content (b) and colority (c) of oxidized maltodextrin (H₂O₂ dosage 40%, catalyst dosage 0.015%).

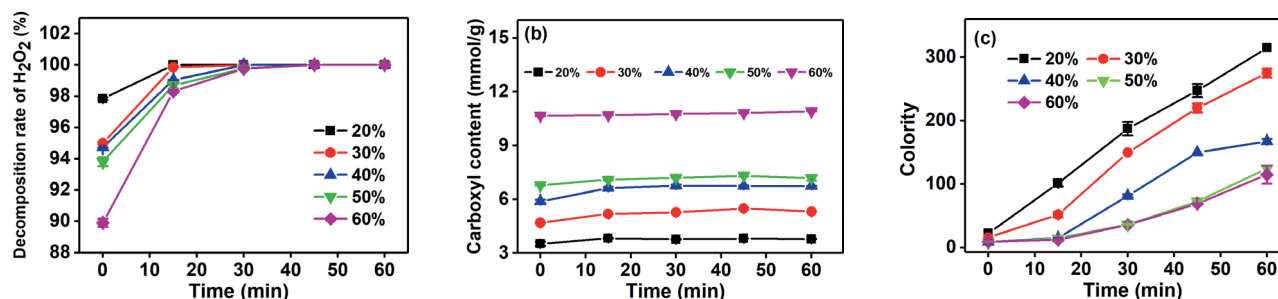


Figure 3. Effects of H₂O₂ dosage on decomposition rate of H₂O₂ (a), carboxyl content (b) and colority (c) of oxidized maltodextrin (catalyst dosage 0.015%, initiation temperature 70°C).

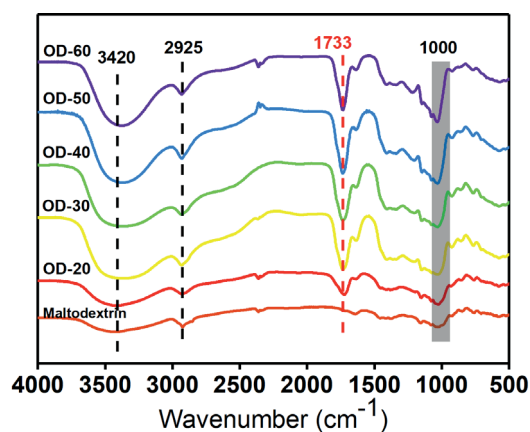


Figure 4. FT-IR spectra of maltodextrin and oxidized maltodextrin with different H_2O_2 dosages.

at 3420 cm^{-1} (stretching vibration of $-\text{OH}$), 2925 cm^{-1} (stretching vibration of $\text{C}-\text{H}$) and band around 1000 cm^{-1} in the fingerprint region ($\text{C}-\text{O}$ and $\text{C}-\text{C}$ bond stretching) suggest the presence of glucosidic ring structure in the oxidized maltodextrin.¹¹

Previous work reported that H_2O_2 can break down the glycosidic bond during oxidation, resulting in the degradation of polysaccharide.²³ The M_w , M_w distribution and average particle size shown in Figure 5 suggest that maltodextrin was also degraded dramatically during oxidation, and the extent of degradation enhanced with the increase of H_2O_2 dosage. In combination of the results in Figure 3, the oxidized maltodextrin with smaller molecular size had higher content of carboxyl groups. To optimize the H_2O_2 dosage and obtain the suitable oxidized maltodextrin ligand for Al–Zr complex tanning, further investigation on the tanning performance will be discussed later.

Tanning Performance

Maltodextrin oxidized by varying H_2O_2 dosages was used as ligand of aluminum–zirconium salts for tanning, and thus the relationship between structure (carboxyl content and molecular weight) and

tanning performance of oxidized maltodextrin can be elucidated. Here we use shrinkage temperature of tanned leather, distribution uniformity of tanning agent, porosity and morphology of leather fiber network to characterize tanning performance (Table III and Figure 6).

The control group without any ligand exhibited much lower results than the groups with ligand (Table III), which reconfirmed that masking agents can promote the penetration and tanning effects of aluminum–zirconium salts. Among the OD groups, OD-40 with moderate carboxyl content (6.75 mmol/g , Figure 3b) and M_w (450) showed better tanning performance. The hydrothermal stability and tanning agent content (shown as metal oxide content) of leather, and distribution uniformity of tanning agent were all higher than those of the other groups, and the extent of fiber dispersion was greater in terms of porosity and SEM analysis showing the fiber network. OD with more carboxyl groups (also lower molecular weight) possessed a stronger complexing effect with Al and Zr ions, leading to the weaker binding ability of metal complexes to collagen fibers at the beginning of tanning. Thus, more uniform penetration and distribution of tanning agent can be achieved. However, too many carboxyl groups on the ligand tend to occupy all the complexing sites of the metal ions and hinder the coordination of the complexes with collagen fiber. This fact can be proven by the decreased metal oxide content of OD-50 (7.21 mmol/g carboxyl, Figure 3b), OD-60 (10.77 mmol/g carboxyl, Figure 3b) and CA (15.62 mmol/g carboxyl) groups compared with OD-40 group, as shown in Table III.

Sufficient tanning effects are supposed to result in satisfactory physical and organoleptic properties of crust leather.¹³ Table IV shows that crust leather from OD-40 group indeed had superior softness and mechanical strengths compared with the other ones. Based on all the results above, OD-40 was chosen as the optimal oxidized maltodextrin ligand for aluminum–zirconium complex tanning.

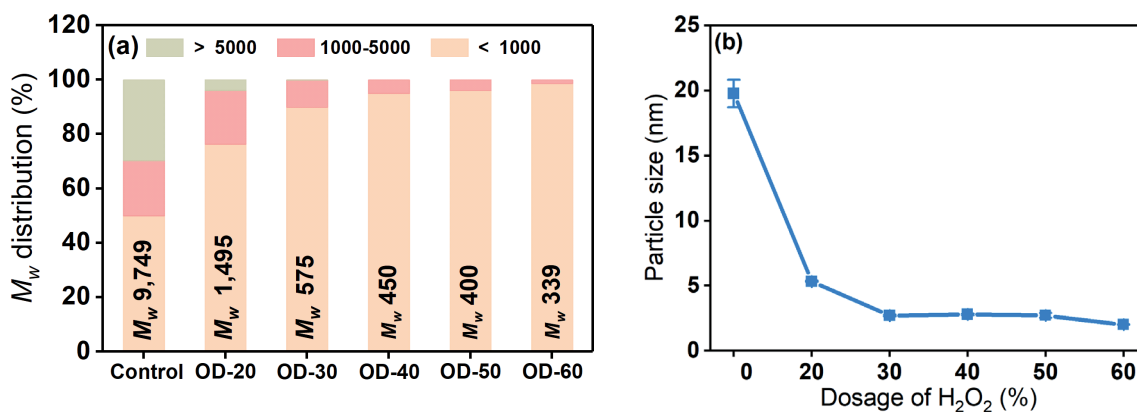


Figure 5. Effect of H_2O_2 dosage on the molecular weight distribution (a) and average particle size (b)

Table III
Properties of tanned leather

Group	Shrinkage temperature (°C)	Distribution uniformity of tanning agent (%)	Metal oxide content (%)	Porosity (%)
Control	75.6 ± 3.1	46.6 ± 1.3	2.2 ± 0.5	48.0 ± 5.9
CA	83.2 ± 0.6	62.8 ± 1.7	2.9 ± 0.1	51.9 ± 0.2
OD-20	80.3 ± 0.2	60.3 ± 2.7	3.8 ± 0.2	50.9 ± 2.2
OD-30	81.8 ± 0.4	70.1 ± 4.5	3.9 ± 0.1	51.2 ± 6.4
OD-40	84.4 ± 0.7	79.2 ± 8.6	4.3 ± 1.6	59.4 ± 7.6
OD-50	81.7 ± 0.6	70.4 ± 12.0	4.3 ± 1.0	53.7 ± 2.6
OD-60	80.1 ± 0.1	73.7 ± 17.0	4.0 ± 1.6	52.7 ± 1.8

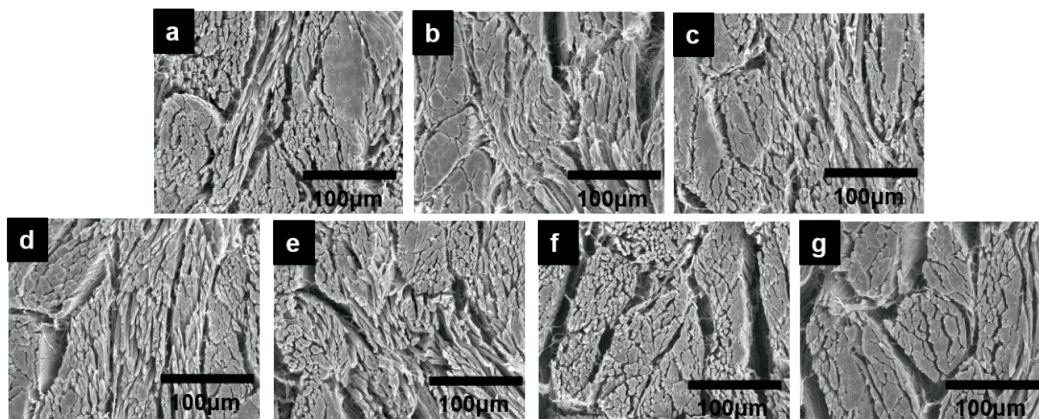


Figure 6. SEM images showing the cross-section of tanned leather (a control, b CA, c OD-20, d OD-30, e OD-40, f OD-50, g OD-60)

Table IV
Physical properties of crust leather

Group	Softness (mm)	Tensile strength (N/mm ²)	Tear strength (N/mm)	Bursting strength (N/mm)
Control	6.9 ± 0.8	13.5 ± 0.1	51.1 ± 4.9	230.6 ± 16.1
CA	6.9 ± 0.8	12.6 ± 1.1	55.3 ± 0.1	246.0 ± 15.7
OD-20	8.2 ± 1.0	13.4 ± 1.0	53.7 ± 4.0	218.7 ± 1.3
OD-30	8.5 ± 0.8	13.3 ± 2.7	57.6 ± 3.6	291.5 ± 11.4
OD-40	9.3 ± 0.3	17.6 ± 3.4	67.2 ± 1.5	300.7 ± 21.2
OD-50	9.1 ± 0.4	16.1 ± 7.6	63.6 ± 4.1	362.2 ± 7.2
OD-60	9.0 ± 0.4	17.2 ± 3.8	69.6 ± 9.2	356.3 ± 7.7

Conclusions

Oxidized maltodextrin with multiple carboxyl groups prepared by H₂O₂ oxidation can be used as a ligand for aluminum–zirconium complex tanning. H₂O₂ dosage played an essential role in the degree of maltodextrin oxidation and degradation. OD-40 (maltodextrin oxidized by 40% H₂O₂) with moderate carboxyl content (6.75 mmol/g) and molecular size (*M_w* 450) exhibited better tanning performance than traditional citric acid ligand, showing its potential application in chrome-free tanning technologies.

Acknowledgement

This work was financially supported by Tianfu Ten-thousand Talents Program and Science and Technology Transformation Project of Deyang City (2020CKC001).

References

- Covington, A. D., Wise, W. R.; Current trends in leather science. *J. Leather Sci. Eng.* **2**, 28, 2020.
- Shi, J. B., Zhang, R. Z., Mi, Z. Y., Lyu, S. Q., Ma, J. Z.; Engineering a sustainable chrome-free leather processing based on novel lightfast wet-white tanning system towards eco-leather manufacture. *J. Clean. Prod.* 124504, 2020.
- Ding, W., Yi, Y. D., Wang, Y. N., Zhou, J. F., Shi, B.; Preparation of a highly effective organic tanning agent with wide molecular weight distribution from bio-renewable sodium alginate. *ChemistrySelect* **3**, 12330-12335, 2018.
- Hedberg, Y. S.; Chromium and leather: a review on the chemistry of relevance for allergic contact dermatitis to chromium. *J. Leather Sci. Eng.* **2**, 20, 2020.
- China, C. R., Hilonga, A., Maguta, M. M., Nyandoro, S. S., Kanth, S. V., Jayakumar, G. C., Njau, K. N.; Preparation of aluminum sulphate from kaolin and its performance in combination tanning. *SN Appl. Sci.* **1**, 920, 2019.
- Ramasami, T., Sreeram, J., Rao, J., Nair, B. U.; Approaches towards elucidating the mechanism of tanning using an organo-zirconium complex. *JALCA*, **95**, 359-367, 2000.
- Wang, Y. N., Huang, W. L., Zhang, H. S., Tian, L., Zhou, J. F., Shi, B.; Surface charge and isoelectric point of leather: A novel determination method and its application in leather making. *JALCA*, **112**, 224-231, 2017.
- Covington, A. D.; Modern tanning chemistry. *Chem. Soc. Rev.* **26**, 111-126, 1997.
- Cai, S. W., Zeng, Y. H., Zhang, W. H., Wang, Y. N., Shi, B.; Inverse chrome tanning technology based on wet white tanned by Al-Zr complex tanning agent. *JALCA*, **110**, 114-121, 2015.
- Sundarrajan, A., Madhan, B., Rao, J. R., Nair, B. U.; Studies on tanning with zirconium oxychloride: Part I: Standardization of tanning process. *JALCA*, **98**, 101-106, 2003.
- Yu, Y., Wang, Y. N., Ding, W., Zhou, J. F., Shi, B.; Preparation of highly-oxidized starch using hydrogen peroxide and its application as a novel ligand for zirconium tanning of leather. *Carbohydr. Polym.* **174**, 823-829, 2017.
- Yu, Y., Wang, Y. N., Ding, W., Zhou, J. F., Shi, B.; Effect of catalyst on structure of hydrogen peroxide oxidized starch and its performance as a ligand in zirconium tanning of leather. *Fine Chemicals*, **35**, 1928-1934, 2018.
- Yu, Y., Zeng, Y. H., Wang, Y. N., Liang, T., Zhou, J. F., Shi, B.; Inverse chrome tanning technology: A practical approach to minimizing Cr(III) discharge. *JALCA*, **115**, 176-182, 2020.
- Huang, W. L., Song, Y., Yu, Y., Wang, Y. N., Shi, B.; Interaction between retanning agents and wet white tanned by a novel bimetal complex tanning agent. *J. Leather Sci. Eng.* **2**, 8, 2020.
- Li, Q., Liu, S., Obadi, M., Jiang, Y., Zhao, F., Jiang, S., Xu, B.; The impact of starch degradation induced by pre-gelatinization treatment on the quality of noodles. *Food Chem.* **302**, 125267, 2020.
- Kutzli, I., Gibis, M., Baier, S. K., Weiss, J.; Electrospinning of whey and soy protein mixed with maltodextrin—Influence of protein type and ratio on the production and morphology of fibers. *Food Hydrocolloid.* **93**, 206-214, 2019.
- Poblete, R., Oller, I., Maldonado, M. I., Luna, Y., Cortes, E.; Cost estimation of COD and color removal from landfill leachate using combined coffee-waste based activated carbon with advanced oxidation processes. *J. Environ. Chem. Eng.* **5**, 114-121, 2017.
- He, X., Wang, Y. N., Zhou, J. F., Wang, H. B., Ding, W., Shi, B.; Suitability of pore measurement methods for characterizing the hierarchical pore structure of leather. *JALCA*, **114**, 41-47, 2019.
- Fu, X., Dai, J., Guo, X., Tang, J., Zhu, L., Hu, C. W.; Suppression of oligomer formation in glucose dehydration by CO₂ and tetrahydrofuran. *Green Chem.* **19**, 3334-3343, 2017.
- Chheda, J. N., Román-Leshkov, Y., Dumesic, J. A.; Production of 5-hydroxymethylfurfural and furfural by dehydration of biomass-derived mono- and poly-saccharides. *Green Chem.* **9**, 342-350, 2007.
- Zhang, Y. R., Wang, X. L., Zhao, G. M., Wang, Y. Z.; Preparation and properties of oxidized starch with high degree of oxidation. *Carbohydr. Polym.* **87**, 2554-2562, 2012.
- Lee, J., Park, S., Roh, H. G., Oh, S., Kim, S., Kim, M., Kim, D. H., Park, J.; Preparation and characterization of superabsorbent polymers based on starch aldehydes and carboxymethyl cellulose. *Polymers-Basel*, **10**, 605, 2018.
- Zhang, S. D., Liu, F., Peng, H. Q., Peng, X. F., Jiang, S. H., Wang, J. S.; Preparation of novel c-6 position carboxyl corn starch by a green method and its application in flame retardance of epoxy resin. *Ind. Eng. Chem. Res.* **54**, 11944-11952, 2015.

Effects of a Clean Subcritical Degreasing System on Wool Fibers

by

Qiao Xia,¹ Yinxuan Wang,² Meina Zhang,² Zongcai Zhang^{1,2*} and Hong Dai^{2*}

¹National Engineering Research Center of Clean Technology in Leather Industry, Sichuan University, Chengdu 610065, P.R. China

²Key Laboratory of Leather Chemistry and Engineering of Ministry of Education, Sichuan University, Chengdu 610065, P.R. China

Abstract

It makes sense to use environmentally friendly methods of degreasing in fur-making process. In this study, subcritical n-pentane was used to degrease wool fibers. Thermogravimetric analysis (TGA) was used to observe and analyze the properties of the subcritical n-pentane degreased wool fibers. The results showed that the thermal stability of the fibers increased. Fourier Transform Infrared (FTIR) spectroscopy was used to analyze the structural changes of macromolecular chains in wool fibers. It was found that when the pressure was higher than 0.4 MPa, the wool fibers underwent a conformational change with the α -helix changing to β -folding. If the pressure was as high as 0.6 MPa, the disulfide bonds in the wool fibers scale layer appeared to break. X-ray powder diffraction experiment was used to study changes in wool fiber aggregation morphology. It was demonstrated that the crystalline zone of wool fibers changed and the fibers index grew, from 22.89% to 30.19%. Field emission scanning electron microscopy and ultra-depth of field microscopy was used to analyze changes in the surface morphology of wool fibers. The results suggested that after the treatment, the wool fibers were not damaged and the impurities on the wool surface were reduced.

Introduction

As we all know, fur is famous for its nobility and elegance, as well as its beautiful appearance. Sheep furs and otter furs are popular with consumers for their relatively low price and excellent warmth. Wool and its products have the following characteristics: practicality, beauty, luxury, value preservation, and sensitivity. In the production of leather, the wools are treated as superfluous and are often removed, resulting in solid waste.¹ However, the removed wool fibers occupy a crucial position in the consumer market. For example, rabbit wools and sheep wools, which are important raw materials for clothing products, are often mixed with man-made fibers and woven into sweaters, where the incorporation of animal wool gives the sweater softness, warmth and lightness. In fact, whether it is rabbit wool or sheep wool, its external structure is a dense layer of scales.² The keratinized cells that make up the scales are arranged in a certain order, forming a dense and strong protective layer on the outside of the wool.³ Due to the presence of the scales, it is difficult

for most foreign substances to enter the interior of the wool, thus it retains good physical and chemical properties such as thermal stability and crystallinity.⁴ In order to satisfy the aesthetics of public consumption, to give the fur products a good feel and to enhance the value of the fur products, large amounts of water is used as a medium to dissolve large amounts of chemical reagents in the fur production process. Wool production wastewater is large in volume, with many types of pollutants, complex composition, high concentration, high chromaticity, and difficult to treat.⁵ In the degreasing process, many degreasers are added to the bath in order to remove excess oil from the wool. These degreasers, which contain high levels of surfactants, are difficult to handle and pose a threat to the environment when discharged into waste water.

Cleaner production is one of the most effective ways to tackle pollution in wool processing. Through the transformation of the wool process, the amount of effluent generated during the production process is reduced at the source. This reduces the investment and running costs of end-of-pipe treatment facilities and eliminates or reduces the risk of products being taken off the market due to environmental problems. At present, subcritical fluid technology has been widely used in the field of cleaner production, such as functional and medicinal plant extraction and production,^{6,7} plant essential oil extraction and production,^{8,9} edible oil extraction and production,^{10,11} plant pigment extraction and production,^{12,13} tobacco industry,^{14,15} textile industry^{16,17} and other industries. The advantages of subcritical extraction processes are as follows. Firstly, the solvent is basically not left behind in the product. Secondly, it does not cause damage to heat-sensitive components in the material. Finally, compared to supercritical extraction technology, large-scale production has been achieved with low investment and low production costs, with the daily processing of 30t of complete sets of equipment only more than 2 million yuan.¹⁸ A few people combine subcritical solvent with wool production and processing. If subcritical fluid can be applied to fur production to replace water as a clean solvent, the wastewater generated in fur production will be greatly reduced.

In a previous paper,¹⁹ subcritical n-pentane was used to degrease sheepskin and its effect on sheepskin was investigated. The results showed that it can remove grease from adipose glands and hair

*Corresponding author e-mail: zhang508@scu.edu.cn, daihong@scu.edu.cn ; first author e-mail: 2392554106@qq.com
Manuscript received December 4, 2020, accepted for publication February 1, 2021.

follicles and it is a clean and efficient degreasing method. So, on this basis, the effect on the wool by subcritical solvent degreasing system was studied further. The degreasing rate of subcritical system applied to wool and the effects of subcritical system on wool thermal stability, aggregation morphology, macromolecular chain structure and surface morphology were mainly studied. It provides feasibility for cleaner production in fur industry.

Experimental

Materials

N-pentane was purchased from Fuchen (Tianjin) Chemical Reagent Co., Ltd. While potassium bromide and alcohol were purchased from Chengdu Changlian Chemical Reagent Co., Ltd. Sheep wool fibers are native of Chengdu.

Sample Preparation

After soaking, flesh was removed from the skin and then the wool was cut off and frozen. Each test consisted of 10g of wool.

The Experimental Process

According to the previous research, it is known that degreasing pressure has a significant influence on the degreasing effect of subcritical n-pentane.¹⁹ Therefore, in these experiments of treating sheep wool fibers with subcritical n-pentane, a representative process condition (degreasing pressure) was selected as a single factor variable. Five different pressures were designed in the experiment: 0.2, 0.3, 0.4, 0.5 and 0.6 MPa. Other degreasing process parameters were as follows: degreasing time 60 min, degreasing temperature 40.5°C, material-liquid ratio 1:7.

The experiment was conducted in a magnetically coupled reactor shown in Figure 1.

Characterization Techniques

Degreasing rate

The degreasing rate was calculated by the following formula:

Where Y is degreasing rate, X_0 represents the oil content of wool fibers before degreasing and X_1 represents the content of removed grease. X_0 is determined by the difference of the mass before and after degreasing. X_1 is determined by Soxhlet extraction.²⁰

$$Y = X_0 / X_1 \times 100\%$$

Change in Thermal Stability in Wool

About 5g samples were weighed and placed in thermogravimetric analyzer (made in Switzerland) for the test at a temperature rise rate of 10°C/min under the condition of nitrogen protection and the temperature range was 150-600°C. During the experiment, the wool fibers were cut into smaller pieces, and then the crucible with wool fibers was put on the balance of the analyzer, and the weight loss of it with the increase of temperature observed. Thermogravimetric analysis (TGA) can accurately measure the process that the mass of the measured substance changes with the change of temperature or time, and is widely used in the research fields of inorganic materials, organic materials, medical drugs and so on.

Structural Changes in Wool Fibers Macromolecular Chains using Fourier Transform Infrared (FTIR) Spectroscopy

In this experiment, the detection parameters of Fourier transform infrared spectrum were as follows: the detection range 4000-400cm, the wave number accuracy 0.01cm, the resolution 0.09cm, the linearity less than 0.07%, and the peak-to-peak noise value better than 5000:1⁻¹. Before analysis and determination, the wool fiber samples were cut into pieces and ground together with potassium

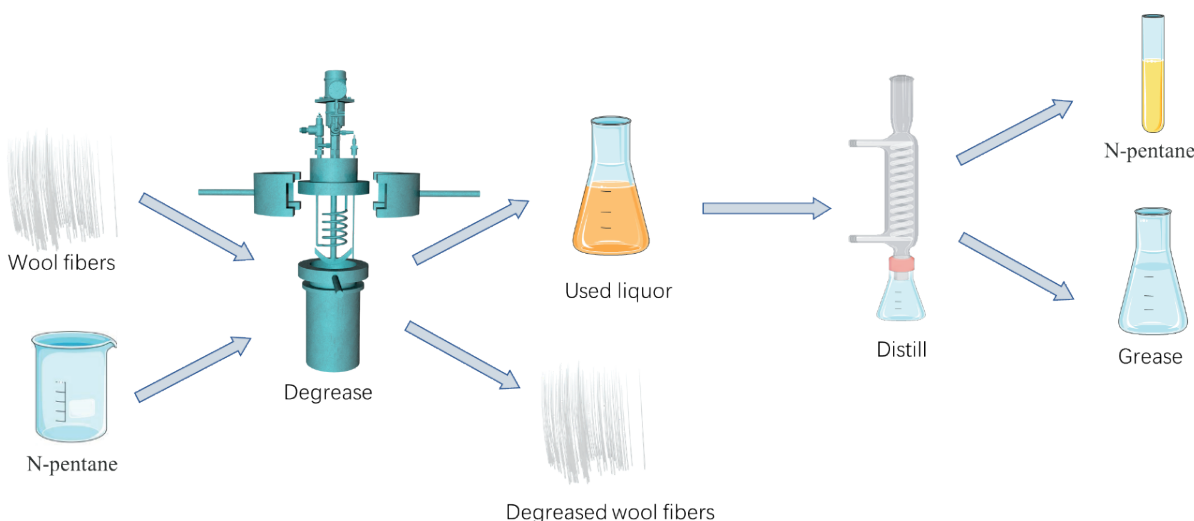


Figure 1. The wool fibers degreasing procedure with subcritical n-pentane.

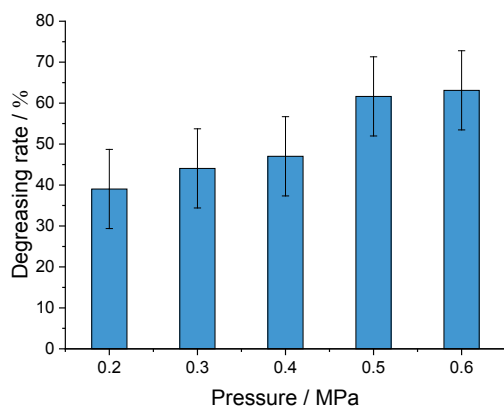


Figure 2. Degreasing rate at different pressures.

bromide powder under the irradiation of a Nernst lamp. After full grinding, the mixture of wool fibers and potassium bromide powder was tabletted, and finally put into a Fourier transform infrared spectrometer for determination.

Structural Changes in the Aggregation State of Wool Fibers using X-Ray Powder Diffraction

X-ray crystallographic analysis was performed on an AXIS Ultra DLD diffractometer (made in The United Kingdom), coupled to a Cu lamp ($\lambda = 1.5405 \text{ \AA}$). The scanning range 5.015-50.000, step size of 0.026° with continuous scanning.

Morphological Changes on the Wool Surface using Scanning Electron Microscopy and Ultra-Depth Microscopy

Field emission scanning electron microscopy (FE-SEM) measurements was performed using a JSM-7500F (made in Japan) instrument. FE-SEM is a widely used analytical instrument, which can explore the surface changes of wool fibers. In the process of experiment, wool fibers were dried by vacuum dryer for 24 h, then gold-plated.

Super-depth microscopic observation was carried out on a VHX-700FC Depth-of-field microscope (made in China).

Results and discussion

Effect of Degreasing

As can be seen from Fig. 2, the degreasing rate of subcritical n-pentane increases with the increase of degreasing pressure. When the degreasing pressure increases from 0.4 MPa to 0.5 MPa, the degreasing rate of subcritical n-pentane improves significantly.

Effect of Subcritical n-Pentane Treatment on Thermal Stability of Wool Fibers

In order to study the influence of subcritical n-pentane on wool fibers, the wool fibers treated with subcritical n-pentane under different pressures were subjected to thermogravimetric analysis with the test temperature ranging from 150°C to 600°C , and the obtained thermogravimetric analysis curves are shown in Fig. 3. The point identified in the figure is the inflection point of weightlessness.

It can be seen from Fig. 3 that the TG curves of wool fibers in the control group and the experimental group can be divided into three stages. In the temperature range from 150°C to 250°C , the weightlessness is mainly due to the volatilization of moisture, perspiration and other components in the wool fibers. During the temperature range from 250°C to 400°C , the weightlessness is mainly attributed to breakage of hydrogen and disulfide bonds in the peptide chain which produces some volatile gases such as H_2S , SO_2 and CO_2 . When the temperature rises above 400°C , the weightlessness is due to the decomposition and consumption of residual carbonized substances in wool fibers.²¹ It can be seen that the inflection point of weightlessness of the treated sample is increased compared with the

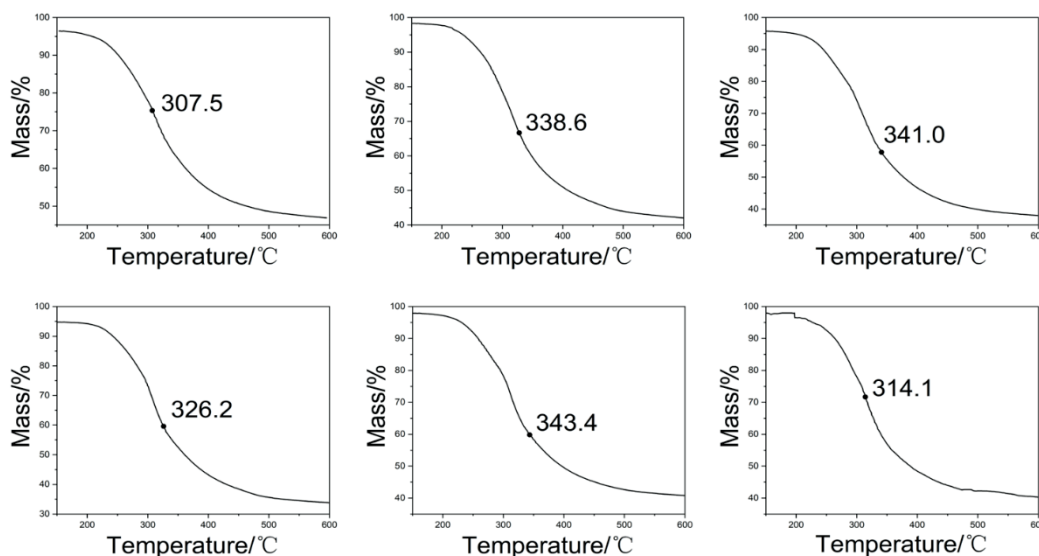


Figure 3. TG analysis curves of wool fibers under different pressures (a, b, c, d, e and f is blank sample, 0.2Mpa, 0.3Mpa, 0.4Mpa, 0.5Mpa and 0.6Mpa).

blank sample. The thermal stability of wool fibers is enhanced after treatment with subcritical n-pentane.

Effect of Subcritical n-Pentane Treatment on Macromolecular Chain Structure of Wool Fibers

In order to explore whether subcritical solvent will affect the interaction between macromolecular segments and the stability of functional groups of wool fibers. Wool fibers treated with subcritical n-pentane under different pressures were selected for Fourier Transform Infrared Spectroscopy (FT-IR) analysis. The abscissa of FT-IR analysis chart is wavenumber, and the ordinate is transmittance T. The formula of light transmittance T is:

$$T = I / I_0 \times 100\%$$

Where I and I_0 are the light intensity of infrared light passing through wool fibers and the light intensity passing through background.

Table I shows the characteristic infrared absorption band of wool fibers. In order to compare the intensity changes of characteristic peaks, several main characteristic peaks were normalized based on

Category	Wavenumber / cm^{-1}	Vibration mode
Hydrogen bond	3300-3500	NH Contraction and Amide II Resonance Absorption
Amide I	1600-1685	C=O stretching region
Amide II	1480-1575	CN and NH stretching
Amide III	1229-1301	CN and NH stretching
Amide IV	625-767	OCN and other kind of stretching

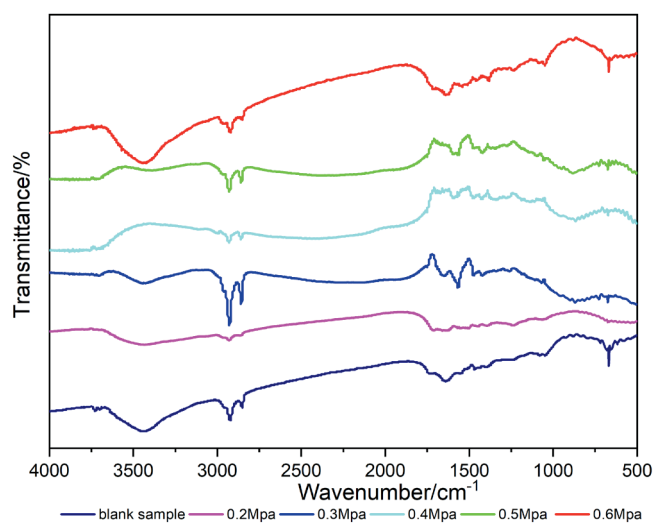


Figure 4. FT-IR analysis of wool fibers at different pressure.

Table II

Relative intensity of some characteristic peaks of wool fibers after subcritical n-pentane treatment at different pressure

Pressure/ MPa	I_{2840} / I_{2990}	I_{1640} / I_{2990}	I_{1240} / I_{2990}	I_{1050} / I_{2990}
Blank sample	1.007	1.040	1.085	1.098
0.2	1.005	1.014	1.030	1.047
0.3	1.002	1.006	1.023	0.990
0.4	1.000	1.018	1.109	1.093
0.5	1.000	1.031	1.087	1.024
0.6	1.010	1.028	1.101	1.112

the absorption peak (C-H) at 2990 cm^{-1} . Table II shows the relative intensity of each characteristic peak after normalization.

Figure 4 shows the infrared spectra of wool fibers treated with subcritical n-pentane under different pressures. Table II shows the relative strength values of each characteristic peak of subcritical wool fibers after normalization. It can be found from Fig. 4 and Table II that the relative intensity of Amide I (C=O) characteristic peak at 1640 cm^{-1} of wool fibers decreased from 1.040 (blank sample) to 1.014 (0.2MPa), 1.006 (0.3MPa), 1.018 (0.4MPa), 1.031 (0.5MPa) and 1.028 (0.6MPa). The results indicated that the effect of C=O bond related to α -helix conformation in wool fibers treated with subcritical n-pentane was weakened. After being treated with subcritical n-pentane at 0.4, 0.5 and 0.6MPa, the relative intensity of Amide III (CN, NH) characteristic peaks at 1240 cm^{-1} of wool fibers increased from 1.085 (blank sample) to 1.109, 1.087 and 1.101 respectively. However, after 0.2 MPa and 0.3MPa subcritical n-pentane treatment, the relative intensity of Amide III (CN, NH) characteristic peaks at 1240 cm^{-1} of wool fibers showed a weakening trend, which decreased to 1.030 and 1.023 respectively. The results indicated that Amide III with β -folding conformation in wool fibers decreased after 0.2 MPa and 0.3MPa subcritical n-pentane treatment, while Amide III with β -folding conformation in wool fibers increased after 0.4 MPa, 0.5 MPa and 0.6MPa subcritical n-pentane treatment. It can be seen that the molecular chain structure of wool fibers changes from α -helix to β -folding after being treated with subcritical n-pentane higher than 0.4MPa. The structural changes are shown in Fig. 5. However, when the treatment pressure is less than 0.4MPa, the molecular chain structure of wool fibers does not change obviously.

At the same time, it can be seen from Table II that the relative intensity of the characteristic peak of S-O in cystine oxide of wool fibers at 1050 cm^{-1} increases from 1.098 (blank sample) to 1.112 (0.6MPa). The related characteristic peak of 2840 cm^{-1} C-H also increased from 1.007 (blank sample) to 1.010 (0.6MPa). It can be seen that when the treatment temperature is as high as 0.6MPa, disulfide bonds in wool fiber scales break and the polarity around $-\text{CH}_2-$ group is enhanced.

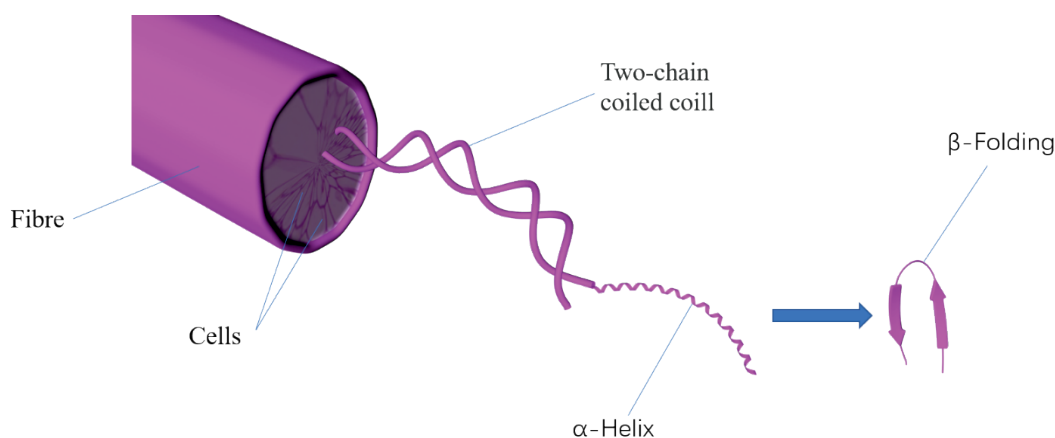


Figure 5. Structural changes of wool fibers.

Effect of Subcritical N-Pentane Treatment on Aggregate Structure of Wool Fibers

In order to analyze the effect of subcritical n-pentane treatment on the aggregated structure (such as crystalline structure and amorphous structure) of wool fibers, wool fibers treated with 0.5 MPa subcritical n-pentane are selected for X-ray powder diffraction analysis. The abscissa of X-ray powder diffraction pattern is diffraction angle 2θ , and the ordinate is diffraction intensity I . The formula of crystallinity C.I. is:

$$C.I. (\%) = \frac{I_{9^\circ} - I_{14^\circ}}{I_{9^\circ}} \times 100\%$$

Where I_{9° and I_{14° are the maximum diffraction intensities of diffraction peaks with diffraction angles 2θ around 9° and $14^\circ 23'$.

Fig. 6 describes the X-ray powder diffraction patterns of wool fibers treated at different conditions. It can be seen from Fig. 6 that there

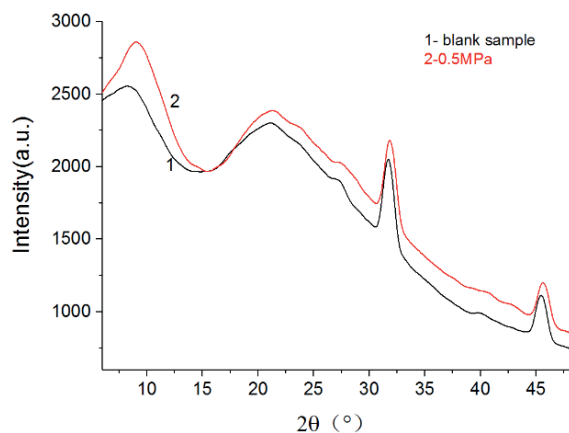


Figure 6. X-ray powder diffraction analysis of wool fibers under different conditions.

are very obvious diffraction peaks near the diffraction angles 2θ of 9° and 20° , which are the common diffraction peaks of α -crystal and β -crystal in wool fibers. Compared with blank samples, the diffraction peak strength of wool fibers treated with 0.5MPa subcritical n-pentane increased at 9° and 20° , and the width of the diffraction peak also widens. The results indicate that the crystal form of the crystalline region of wool fibers changed after 0.5MPa subcritical n-pentane treatment, and the α -crystal changed into β -crystal.

Table III shows the change of crystallization index of wool fibers after treatment under different conditions. It can be seen from Table III that the crystallization index of wool fibers increased from 22.89% to 30.19%. Therefore, after treatment with subcritical n-pentane, the α -crystal and β -crystal crystallization in wool fibers increased and the crystallinity of wool fibers significantly improved.

Table III
Crystallization index of wool fibers
under different conditions

Condition	$I_{9.0^\circ}$	$I_{14.1^\circ}$	C.I.
Blank sample	2534	1954	22.89%
0.5 MPa	2875	2007	30.19%

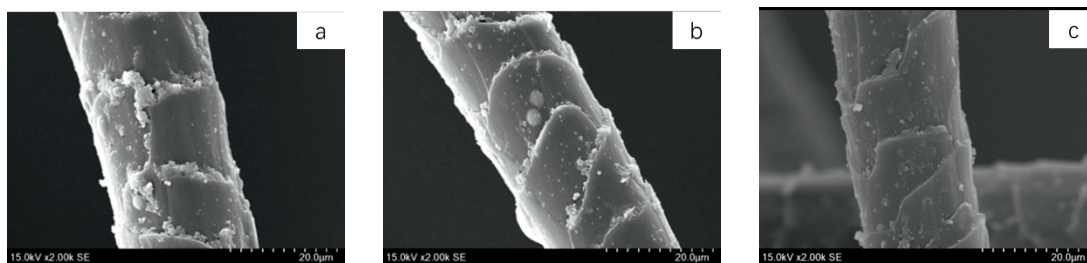


Figure 7. SEM micrographs of wool fibers under different pressures (a, b and c represent wool fibers before treatment, after 0.2 MPa subcritical n-pentane and 0.6 MPa subcritical n-pentane).

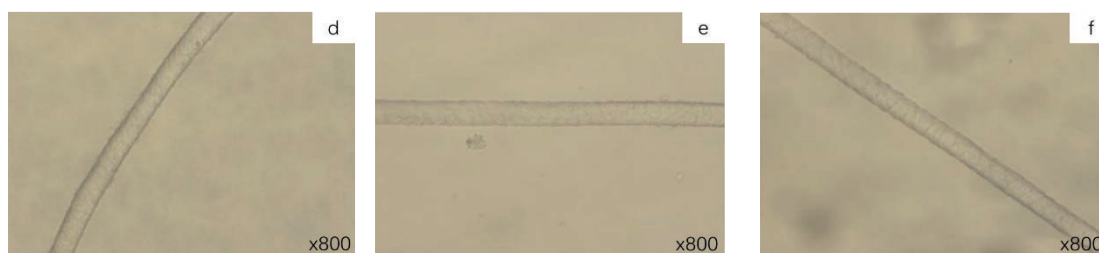


Figure 8. VHX micrographs of wool fibers under different pressures (d, e and f represent wool fibers before treatment, after 0.2 MPa subcritical n-pentane treatment and 0.6 MPa subcritical n-pentane)

Effect of Subcritical N-Pentane Treatment on Wool Surface Morphology

In order to investigate the effect of subcritical n-pentane on the surface morphology of wool fibers, wool fibers treated with 0.2 and 0.6 MPa subcritical n-pentane are selected for scanning electron microscope and super depth of field microscope. The observation results are shown in Fig. 7 and Fig. 8.

It can be seen from Fig. 7 and Fig. 8 that the scales covered by wool fibers before treatment are thick, arranged and complete in shape. Some impurities are attached to the scales. It can be seen from the graph that the subcritical treatment did not cause significant damage to the wool fibers. However, the impurities on the wool fibers were decreased, indicating that subcritical n-pentane can remove the impurities from the wool surface.

Conclusion

The results show that subcritical n-pentane is an environmentally viable degreaser and the degreasing rate increases with increasing pressure. After subcritical n-pentane treatment, wool fibers showed the following changes: The thermal stability of wool fibers improved. If the pressure was higher than 0.4 MPa, the wool fibers underwent a conformational change from the α -helix to β -folding. When the pressure reached 0.6 MPa, the disulfide bond broke. After 0.5 MPa of subcritical n-pentane treatment, the crystallization pattern of

wool fibers crystallization zone changed from α -crystal to β -crystal, and the crystallization index increased from 22.89% to 30.19%. The subcritical treatment does not damage the wool and also removes impurities from the surface of the wool.

Acknowledgement

We acknowledge the financial support provided by Ningxia Hui Autonomous Region Key R&D Projects (2019 BFH2007).

References

1. Yanchun Li, Ruijun Guo, Wenhui Lu and Deyi Zhu. Research progress on resource utilization of leather solid waste. *Journal of Leather Science and Engineering*, **1**:6, 2019.
2. He Yujie. Structural Characterization and Analysis of animal fibers *J. Textile Report*, **05**, 31-32, 2017.
3. Fengxiang Luo, Xiang Zhong, Mengchu Gao, Biyu Peng, Zhongzhen Long. Progress and mechanism of breaking glycoconjugates by glycosidases in skin for promoting unhairing and fiber opening-up in leather manufacture. A review. *Journal of Leather Science and Engineering*, **2**:12, 2020.
4. Jie Liu, Lan Luo, Yadi Hu, Fang Wang, Xuejing Zheng and Keyong Tang. Kinetics and mechanism of thermal degradation of vegetable-tanned leather fiber. *Journal of Leather Science and Engineering*, **1**:9, 2019.

5. Hua Jinling, Cheng Fengxia, Dong Ronghua, Xu Ransong, Zhou Yongxiang. Analysis on the characteristics and treatment status of fur production wastewater *J. China leather*, **21**,55-58, 2008.
6. Hofstetter Robert K, Potlitz Felix, Schulig Lukas, Kim Simon, Hasan Mahmoud, Link Andreas. Subcritical Fluid Chromatography at Sub-Ambient Temperatures for the Chiral Resolution of Ketamine Metabolites with Rapid-Onset Antidepressant Effects. *J. Molecules* (Basel, Switzerland), **24**(10), 2019.
7. Drugs and Therapies - Antioxidants; Researchers at Chinese Academy of Sciences Target Antioxidants (Subcritical fluid extraction of Lycium ruthenicum seeds oil and its antioxidant activity) *Food Weekly News*, 2019.
8. Cristiana Radulescu, Radu Lucian Olteanu, Claudia Stih, Monica Florescu, Raluca Maria Stirbescu, Sorina Geanina Stanescu, Cristina Mihaela Nicolescu, Marius Bumbac. Chemometrics-based vibrational spectroscopy for *Juglandis* semen extracts investigation, *Journal of Chemometrics*, **34**(6), 2020.
9. Zhao Ying, Fan Yang-Yang, Yu Wen-Gang, Wang Jian, Lu Wenju, Song Xi-Qiang. Ultrasound-Enhanced Subcritical Fluid Extraction of Essential Oil from *Nymphaea alba* var and Its Antioxidant Activity, *Journal of AOAC International*, **102**(5), 2019.
10. Zanqui Ana Beatriz, de Moraes Damila Rodrigues, da Silva Claudia Marques, Santos Jandyson Machado, Gomes Sandra Terezinha Marques, Visentainer Jesuí Vergílio, Eberlin Marcos Nogueira, Cardozo-Filho Lúcio, Matsushita Makoto. Subcritical extraction of flaxseed oil with n-propane: Composition and purity, *Food Chemistry*, **188**, 2015.
11. Claudia Marques da Silva, Ana Beatriz Zanqui, Jesuí Vergílio Visentainer, Lúcio Cardozo-Filho, Paulo Rodrigo Stival Bittencourt, Damila Rodrigues Moraes, Jandyson Machado Santos, Marcos Nogueira Eberlin, Makoto Matsushita. Quality and composition of three palm oils isolated by clean and sustainable process *Journal of Cleaner Production*, **259**, 2020.
12. Nur Azzanizawaty Yahya, Nursyafreena Attan, Roswanira Abdul Wahab. An overview of cosmeceutically relevant plant extracts and strategies for extraction of plant-based bioactive compounds, *Food and Bioproducts Processing*, **112**, 2018.
13. Lu Jie, Feng Xiaomei, Han Yuqian, Xue Changhu. Optimization of subcritical fluid extraction of carotenoids and chlorophyll a from *Laminaria japonica* Aresch by response surface methodology, *Journal of the Science of Food and Agriculture*, **94**(1), 2014.
14. Zhang Sheng, Wu Changwei, Liu Yuyu, Read Xiaoki, Li Xian. Subcritical preparation of tobacco extract and its application in cigarettes, *Food Industry*, **34**(12):31-33, 2013.
15. Yang Jun-peng, WANG Shan, ZHOU Hong-yin, WANG Hao. Preparation of tobacco flavoring by molecular distillation of clove subcritical extract, *Yunnan Chemical Industry*, **47**(04), 64-66, 2020.
16. Chen Miaoyuan, Gu Lingbiao, Lu Keke, Kong Lingjun, Liu Huamin, Pang Huili, Qi Kun, Zhu Xinliang, Qin Guangyong. Optimization of subcritical lanolin extraction process by response surface method, *Chinese Journal of Textiles*, **36**(12), 69-74, 2015.
17. Niu Zhenhuai. Research on recycling of waste polyester fabric, *Taiyuan University of Technology*, 2015.
18. Qi Kun. Development and status of subcritical solvent biological extraction technology, *Grain and Food Industry*, **19**(05), 5-8, 2012.
19. Qiao, X.; Meina, Z.; Bo, M.; Hong, D.; Zongcai, Z. Study on the Degreasing of Sheep Skin Using Subcritical Fluid Extraction, *JALCA* **116**(2), 2021.
20. ISO 4048:2018 Determination of matter soluble in dichloromethane and free fatty acid content.
21. Li Zhi, Liu Huimin, Wu Weihong, Zhang Dongnuan, Song Lili, Wang Junmin. Study on thermal properties of flame retardant wool fiber, *Journal of Hebei University (Natural Science Edition)*, **04**, 386-390, 2005.
22. Chen Liping. Structural analysis of wool keratin membrane, *Chinese Society of Textile Engineering*, 229-232, 2009.
23. Zavadskii A E. X-ray diffraction method of determining the degree of crystallinity of cellulose materials of different anisotropy, *Fibers Chemistry*, **36**(6), 425-430, 2004.

Learning to Recognize Irregular Features on Leather Surfaces

by

Masood Aslam,¹ Tariq M. Khan,^{2*} Syed Saud Naqvi,¹ Geoff Holmes³ and Rafea Naffa³

¹*Department of Electrical and Computer Engineering, COMSATS University Islamabad, Islamabad Campus, Islamabad 45550, Pakistan*

²*School of Information Technology, Deakin University, Geelong, VIC 3217, Australia*

³*NZ Leather and Shoe Research Association (LASRA), Palmerston North 4414, New Zealand*

Abstract

As part of industrial quality control in the leather industry, it is important to identify the abnormal features in wet-blue leather samples. Manual inspection of leather samples is the current norm in industrial settings. To comply with the current industrial standards that advocate large-scale automation, visual inspection based leather processing is imperative. Visual inspection of irregular surfaces is a challenging problem as the characteristics of the abnormalities can take a variety of shape and color variations. The aim of this work is to automatically categorize leather images into normal or abnormal by visual analysis of the surfaces. To achieve this aim, a deep learning based approach is devised that learns to recognize regular and irregular leather surfaces and categorize leather images on its basis. To this end, we propose an ensemble of multiple convolutional neural networks for classifying leather images. The proposed ensemble network exhibited competitive performance obtaining 92.68% test accuracy on our own curated leather images dataset.

1 Introduction

In the production of high quality wet-blue leather, automation of defect inspection and classification is highly desirable. Inspection is carried out at different stages of production. It is clear that more leather abnormalities can be prevented by earlier identification. To date, the industry's inspection of abnormal leather surfaces relies primarily on human vision. However, because of human error, manual inspection is strongly subjective, which could eventually lead to low productivity and an undesired false detection rate. With the developments of artificial intelligence (AI) in recent years, its practical applications in visual-based detection in many industrial sectors have been successfully demonstrated.¹⁻³ Also, with the rise of industry standard 4.0,⁴ AI based visual inspection of leather samples is imperative.

Visual inspection based leather categorization is a challenging problem as the appearance of the irregularities is highly varying in nature. Hides and skin defects are usually known as antemortem (before animal death), post-mortem (fault after animal death) and

as defects of processing. Brand marks, pox marks, tick marks, insect bites, bruises, growth marks, scratches, etc. are potential defects that arise during the animals' lifespan. These defects are distinguished by a range of shapes, colors, and textures. The data shift problem on the test set and similar visual appearance of normal and irregular leather surfaces further make the problem multifaceted.

AI deals with developing theory, methods and systems that can enable machines to mimic human intelligence. Neural networks are a small step in this direction that attempt to mimic the human brain and its functionality. The area of artificial intelligence which deals with imitating the behaviour of human vision is image processing. While other AI techniques have also played their roles, neural networks have come a long way in replicating simple human vision tasks including handwritten digit recognition, number plate reading and visual recognition.⁵ Neural networks have demonstrated their efficacy on a wide range of image processing applications including image enhancement, compression, image segmentation, object recognition and image understanding.⁵

In the past non neural network based AI methods have been investigated for visual inspection of leather.^{6,7} While they achieve considerable performance, the current state of methods is far from reaching a generic solution that can meet the needs of industrial scale visual inspection. Moreover, convolutional neural networks (CNN) based methods (that are a special type of neural networks) have not been explored to their fullest potential for visual inspection of leather. A valid reason for this is the lack of data sets which is a major impediment to progress in this area. The previous studies do not make their data available for comparative evaluation.

The aim of this paper is to design a system capable of automatic classification of leather images as normal or flawed. The proposed system can be easily adapted to automated leather hide categorization by leveraging its robust image-by-image classification capability. Such a system can act as a support system for the experts and aid in bias free, rapid categorization of leather samples. The major objectives to achieve the aim of the paper are as follows:

- systematic ensembling of state-of-the-art CNNs and their adaptation for leather image categorization,
- comparative evaluation of the proposed method with previous state-of-the-art machine and deep learning based approaches in terms of widely accepted classification performance metrics,
- introduce a high resolution, wet-blue leather image dataset for benchmark comparative evaluation of methods.

In this work, we propose an ensemble convolutional neural network that is designed systemically through empirical evaluations for robust leather sample categorization. We also introduce a new high-resolution wet-blue leather image dataset consisting of normal and defective leather samples. The images are acquired in a controlled environment with a digital camera device. The major challenges in image acquisition using a digital camera device include proper illumination conditions, proper distance from the leather surface and managing the field of view and ensuring high resolution of images. Other important factors are stability of the acquisition device to exclude the possibility of image artefacts. The dataset introduced in this work was curated by taking into account all the above-mentioned issues.

The major contributions of the proposed work are:

- a new ensemble method for robust leather sample classification,
- a thorough comparative evaluation of the proposed method with nine benchmark machine and deep learning based methods,
- introduction of a new high-resolution leather images dataset for stimulating research in the field.

As explained earlier, wet-blue leather has multiple types of defects, however, in this work we are only interested in classifying leather images as normal or abnormal. In this paper, we will use the terms defects and irregular features interchangeably for abnormal leather surface regions (i.e., cuts in our case). The visual appearance of these abnormal image regions is characterized by a wide variety of shapes, textures, scales, spatial locations, and color variations.

The rest of the paper is organized as follows. Section 2 contains a literature review on leather defect classification. Section 3 describes the proposed method. Section 4 explains experimental design. In section 5 all results are presented. Class Activation Maps are explained in section 6. Finally, we conclude our work in section 7.

2 Literature Review

In this section, we review several machine learning based methods proposed in the literature for leather image classification. To identify abnormal features, Chishti et al. proposed LM-trained multi-layer

perceptron neural network structure optimization algorithms have been developed. The suggested results of the method have better accuracy than existing LM-based classifiers without neural structure optimization. Dataset images for wet blue leather and rawhides of the 11 most common features are provided with the classifier results. The algorithm classifies wet blue leather defects with 98.73% accuracy, 97.85% precision, and 94.14% sensitivity.⁶ Deng et al. proposed a method to classify surface abnormalities on the whole piece of the leather automatically and objectively, based on a parameter optimized residual network is proposed. They used ResNet-50 and optimized two of the network parameters, the size of the data set and the size of the sliding patch window, are optimized. The size of the data set is obtained by achieving the tradeoffs between the evaluated workload and the classification accuracy. The classification accuracy of the applied reaches 94.6%.⁷ Recently, Aslam et al. suggested a method to classify good leather and defected leather images. For the classification task, an ensemble architecture EfficientNet-B3+ResNext-101 is used. The proposed algorithm was able to achieve an AUC of 81.9%.⁸

3 The Proposed Method

In this work, we investigated deep learning architectures for classification of abnormal surface features in wet-blue leather. Images were acquired using a Nikon Coolpix P300 camera. Training images were employed to augment new image variations to improve the generalization of classifiers on unseen samples. The classifiers were trained using augmented data and train and validation accuracies were computed. The best weights of the trained models were stored for the inference stage. In the inference stage, the test data and the chosen trained model was employed to compute the model predictions, which were then utilized for performance evaluation of the model at the test stage.

3.1 Data Augmentation

In order to train the network with different variations of the input images by artificially generating new images for the training, the data augmentation module was added to our workflow. In order to minimise network overfitting and enhance model generalisation, the data augmentation effect has been practically demonstrated.

Horizontal flipping, vertical flipping, rotation using a random angle in the range 30 to 150 and a random zoom factor in the range 0.1 to 0.8 were the chosen augmentation methods in our experiments. With a probability of 0.5, all the transformations were applied. After the data augmentation process, a total of 1557 images were collected. The training data was split randomly into training, validation and test sets with a 60:20:20 ratio. Consequently, for the training collection, 1040 images were used, while the remainder were split into the validation and test sets. The number of defective and non-defected pictures of leather were also held equal, rendering the issue of classification a balanced one. Apart from data augmentation

strategies, no particular pre-processing function was applied to the original images.

3.2 Convolutional Neural Network Ensembles

Ensemble approaches combine several classifiers, and it has been found that it is possible to obtain greater precision results than a single classifier. For an ensemble, well-known approaches include boosting, bagging and stacking. Stacking combines the outputs of a number of base learners and allows another algorithm, called the meta-learner, to make the final predictions. A super-learner is another technique which calculates the final predictions by finding the optimal weights of the base learners by minimising a loss function based on the cross-validated performance of the learners. Majority voting is an ensemble method that counts all the predicted labels of the base learners, and records the label with the highest number of votes as the final prediction. Another strategy is to measure the optimum weights of individual simple learners. Average voting that produces labels afterwards by calculating the average probabilities of the softmax class or predicted labels for all the base learners is the most common ensemble technique used in neural networks.

In this work, we experimented with various combinations of standard state-of-the-art networks, including VGG-16, ResNet-50, Inception-V3 and Inception-ResNet-V2, in order to find the ideal collection for classifying leather features. The average voting-based ensemble of Inception-V3+ResNet50 was selected as the proposed architecture in this study due to its superior performance and confidence in predictions. The architectural level diagram of the proposed ensemble network is shown in Figure 1.

Ensemble techniques have proven in previous works to be the tool of choice in both related and unrelated image domains. Ensemble approaches combine several classifiers, and it has been found that it is possible to obtain greater precision results than a single classifier. We put together state-of-the-art designs such as Inception-V3, VGG-16, ResNet-50 and Inception-ResNet-V2. Since no representative ensemble methods are discussed for leather image classification

in literature, ensemble combinations of two network architectures are exhausted and combinations are chosen in this work that stand out in terms of learned representations. For related domain classification tasks, similar ensemble networks have demonstrated state-of-the-art efficiency. Neural networks are nonlinear and have a high variance, ensemble learning combines the predictions from various architectures to reduce variance of prediction.

Figure 1, consists of two different convolutional neural network architectures, i.e. ResNet-50 and Inception-V3. Input image is fed separately to both the models. Both networks have a Global Average Pooling (GAP) layer as their outputs (for details about GAP, please refer to Section 3.4). In order to calculate the final prediction, the outputs of the networks are fed into the probabilistic averaging layer. The output of the probabilistic averaging layer is passed through a softmax layer that categorizes the input image as normal or defective.

3.3 Setting Up the CNN and Training Process

Our model was implemented using Keras deep learning framework 2.1.4. Stochastic Gradient Descent (SGD) and the ADAM optimizers were investigated.^{9,10} The momentum rate equal to 0.9 for SGD and set the learning rate to 0.001. We adopted a dynamic learning rate which was divided by 1×10^{-3} every epoch with an initial value of 1×10^{-2} for Inception V3 experiments. The training batch size used for Inception-V3+ResNet-50 was 4. We used a binary cross entropy as loss function denoted by L_{CE} because there are only two classes.¹¹ The subscript in L_{CE} stands for cross entropy. Our loss function takes the following form

$$L_{CE}(y, \hat{y}) = -\frac{1}{N} \sum_{i=0}^N (y_i \log(\hat{y}_i) + (1 - y_i) \log(1 - \hat{y}_i)) \quad (1)$$

where y is the label, \hat{y} denotes the predicted probability and \log is the natural logarithm.

All images in the dataset were re-sized to 500×375 pixels before training the CNN model to preserve the information in the image and reduce the computational cost of processing. Hence, the input

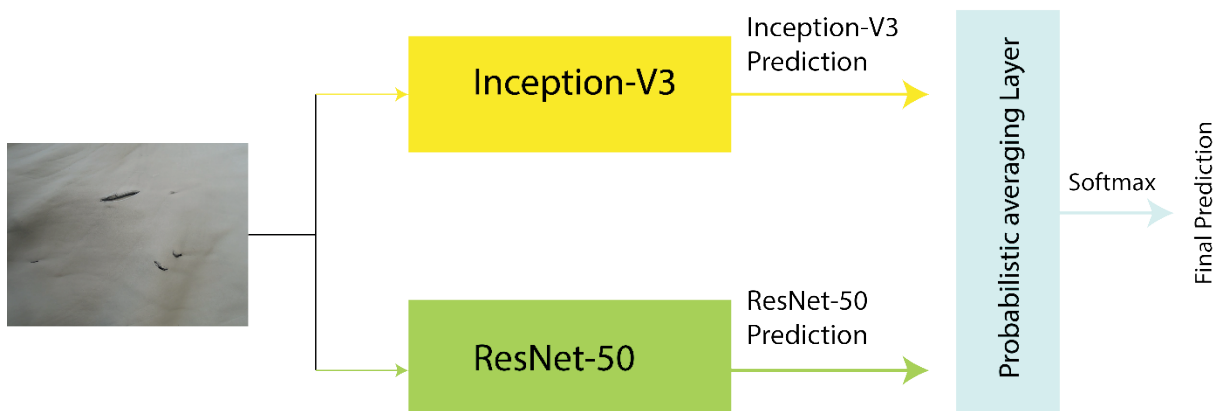


Figure 1. Block level diagram of the proposed ensemble architecture.

Table 1
Comparison of models parameters with and without the GAP layer.

Serial #	Model	Original Parameters	Parameters with GAP
1	Inception-V3	23 Million	21.8 Million
2	Inception-ResNet-V2	55 Million	54 Million
3	ResNet-50	25 Million	23 Million

shape of the CNN is $500 \times 375 \times 3$, where three represents the number of RGB channels in the image. We employed the pre-trained weights on ImageNet for the convolutional blocks as an initialization for the network parameters, which resulted in a faster convergence.¹² We also added Global Average Pooling layer and replaced dense layer and flatten layer. The elimination of all these trainable parameters also reduces the tendency of over-fitting, which needs to be managed in fully connected layers by the use of dropout.

3.4 Global Average Pooling

One of the most important requirements for visual inspection based leather defect categorization is the large size of the input images. Large image sizes are essential as irregular features can occur at very small scales and equally contribute to the defectiveness of the leather sample. Therefore, the CNN architectures designed for this task must be able to cope with large image sizes. This large image size support is not very common in state-of-the-art CNNs reported in literature for classification tasks. It turns out that large image sizes can only be supported by models that have a relatively lower number of parameters. One such recent state-of-the-art architecture, which has proven to be highly useful at the large scale visual recognition challenge and has an architecture targeted to mobile vision is the Inception-V3 architecture.¹³ The Inception-V3 is a well-known state-of-the-art method for multi-class classification with a low computational cost and only consists of 25 million parameters.¹³ The ResNet-50 architecture can be carefully optimized to minimize the number of parameters without compromising its established state-of-the-art classification performance in related tasks.

Despite its low computational cost, the proposed Inception-V3+ResNet-50 architecture could not be trained in an end-to-end fashion on leather images greater than $500 \times 375 \times 3$ using a multi-gpu hardware resource. To counter this issue, we considered various global pooling layers instead of the fully connected layer to reduce the number of parameters and shed the computational load. Table 1 presents a comparison of model parameters, where the original parameters depict the total parameters (with the fully connected layer), while the parameters with GAP represents the total number of model parameters when the GAP layer is employed. If we look at Inception-V3 parameters, the number of parameters are reduced by about 1 million. Also, in the case of Inception-ResNet-V2, the

difference is about 1 million as well. In ResNet-50 the difference is 2 Million parameters, which is slightly more than Inception-V3 and Inception-ResNet-V2.

Four well-known pooling strategies from past works including simpler schemes such as global max pooling,¹⁴ global average pooling,¹⁵ and more complex strategies including log sum exponential (LSE) pooling¹⁶ and max-min pooling¹⁷ were considered. Considering that V^c represents a map from the final convolutional volume of the architecture, we can define all the pooling strategies. The global max pooling strategy denoted by y^cM as defined in,¹⁴ is given as:

$$y^cM = \max_{i,j} V_{ij}^c \forall c \in C \quad (2)$$

Where C represents the number of scores in map and c is the maximum score in that map. The maximum location in the map hypothetically provides the location of the object or the abnormal region in our case.

Similarly, global average pooling (denoted by y^cA), which is another simple pooling scheme, can be defined according to¹⁵ as

$$y^cA = \frac{1}{N} \sum_{i,j} V_{ij}^c \quad (3)$$

Where N is the total number of samples, V^c represents a map from the final convolutional volume of the architecture. It advocates that the location of the region of interest is the global average of the maps instead of the maximum as in global max pooling.

Given a hyperparameter β , the LSE pooling strategy¹⁶ (denoted by y^cLSE) can be expressed as

$$y^cLSE = \frac{1}{\beta} \log \left(\frac{1}{N} \sum_{i,j} \exp(\beta V_{i,j}^c) \right) \quad (4)$$

where β provides a trade-off between choosing the maximum versus the average values for pooling, \log is the natural log and \exp represents the exponential function. In some sense, the LSE pooling strategy provides as trade-off between the global average and max pooling strategies to locate the object of interest. Finally, the min-max pooling strategy based on the k highest ($S_{top}(V^c)$) and the m lowest ($S_{low}(V^c)$) scoring regions is expressed mathematically according to¹⁷ as

$$y^cMax - Min = S_{top}(V^c) + S_{low}(V^c) \quad (5)$$

$$S_{top}(V^c) = \max_{i,j} h \sum_{i,j} h_{ij} V_{ij}^c, \text{ s.t. } \sum_{i,j} h_{ij} = k \quad (6)$$

$$S_{low}(V^c) = \min_{i,j} h \sum_{i,j} h_{ij} V_{ij}^c, \text{ s.t. } \sum_{i,j} h_{ij} = m \quad (7)$$

where \mathbf{h} is a vector responsible for the selection of the candidates. The main idea of the max-min pooling strategy is that multiple regions

Table II
Computational complexity of pooling strategies

Pooling Strategy	Proposed by	Big-O complexity
Global max pooling y^cM	Oquab et al. ¹⁴	$O(n^2)$
Global average pooling y^cA	Zhou et al. ¹⁵	$O(n)$
LSE pooling y^cLSE	Pinheiro et al. ¹⁶	$O(\log(O(k(O(n))))))$
Max-min pooling $y^cMax-Min$	Durand et al. ¹⁷	$O(2n) \rightarrow O(lp)$

that hypothesize the location of the object of interest are combined to form the final prediction.

Two important factors that need to be considered when selecting a pooling strategy are the accuracy of the network and the computational overhead of the scheme. In our experiments, all four pooling strategies obtained relatively similar results in terms of accuracy, therefore, we considered computational complexity of the operations to select a particular pooling scheme. Table II, presents the computational complexity of the pooling strategies considered in this work. As the more complex LSE and Max-min pooling schemes have relatively much higher computational complexity with almost similar accuracy as compared with the other two schemes, the simple max and average pooling schemes were considered in this work. Owing to its higher accuracy in our experiments and lower computational complexity according to

Table II, global average pooling (GAP) y^cA was considered to be the preferred choice. The overall complexity of the max-min pooling strategy is $O(2n^2)$, however, the parameter h needs optimization, which adds a term $O(lp)$ for each optimization iteration for p number of derivatives.

4 Experimental Design

4.1 Dataset

The original dataset consists of RGB wet-blue leather images with a resolution of 4000×3000 in JPEG format. The images were collected by Nikon Coolpix P300 camera with a 12MP AF sensor. A total of 60 images including 30 normal samples and 30 defected samples were curated to form the original dataset. Equal representation of normal and defective samples was collected to balance the classes. The original images were augmented as explained in Section 3.2 to form a total of 1557 images, out of which, 1040 images were used for training and the rest constituted the validation and test sets.

Figure 2 presents representative examples of normal and defective images along with magnified regions of abnormal and normal leather surfaces. Abnormal or irregular leather surfaces are distinguishable from a normal surface based on the color, texture and shape of the defects characterizing them. For instance, the abnormal surfaces shown with red boxes in Figure 2 contain cuts and white spots, which are highly varying in appearance due to their color, texture and shapes.

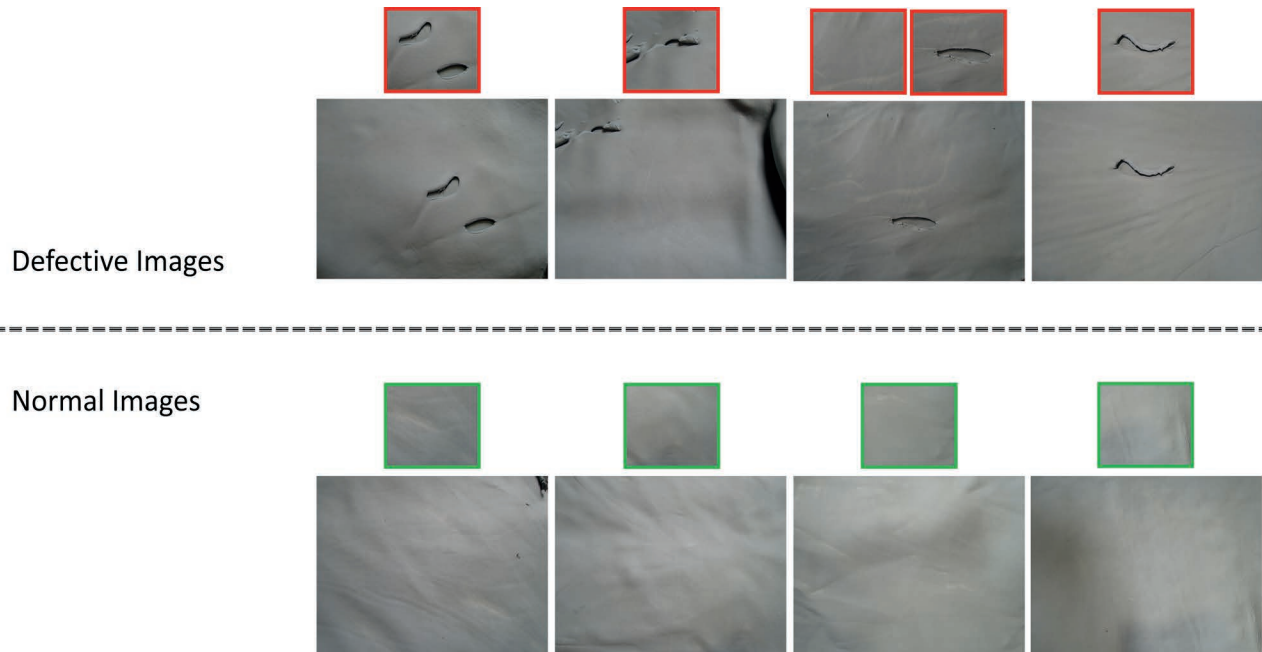


Figure 2. Representative examples of defective and normal images. Image patches on top of the images show abnormal (red boxes) and normal (green boxes) leather surfaces, respectively.

4.2 Performance Measures

When performing classification predictions, four types of outcomes could occur:

- **True Positive (TP):** When a defected leather sample is predicted as defected by the model,
- **True Negative (TN):** When a leather sample without any defects is predicted as non-defected by the model,
- **False Negative (FN):** When defects were present in leather but the model predicted it as non-defective; it is also called as a Type 2 error,
- **False Positive (FP):** When the leather sample was non-defective but the model predicted it as defective; it is also known as a Type 1 error.

Several different performance measures based on the confusion matrix are employed to assess the classification performance of the methods. These measures include the classification accuracy that measures the percentage of correct predictions

$$\text{Accuracy} = \frac{TP + TN}{TP + FP + TN + FN} \quad (8)$$

As per equation (8), it is computed by dividing the number of correct predictions by the number of total predictions. The accuracy measure computed for the training images is termed as the train accuracy. Accuracy for the validation images is the validation accuracy and the accuracy computed on the test image set is known as the test accuracy.

The precision of the classifier quantifies what proportion of positive predictions were deemed correct and is given as

$$\text{Precision} = \frac{TP}{TP + FP} \quad (9)$$

A related measure is recall which measures the proportion of actual positives which were identified correctly

$$\text{Recall} = \frac{TP}{TP + FN} \quad (10)$$

The F1-score is the average of the precision and recall

$$\text{F1 - score} = 2 \frac{\text{Precision} \times \text{Recall}}{\text{Precision} + \text{Recall}} \quad (11)$$

A Receiver Operating Characteristic (ROC) curve is a fundamental method to evaluate the classifier's test assessment for various classification thresholds. A plot between the sensitivity (true-positive rate) as a function of the specificity (false-positive rate) is shown in this curve for different parameter threshold values. Each point on the graph in the ROC plot is a pair of FPR and TPR values

for a particular threshold point. The AUC therefore reflects how a classifier distinguishes between flawed and non-defect leather.

4.3 Benchmark Deep Learning Methods

To this end, we employ ResNet, inception-V3 and Inception-ResNet-V2 as benchmark deep learning based methods for comparative evaluation of the proposed method. The VGG16 method is employed as the baseline method for comparison. ResNet has several architectures with different number of layers.¹⁸ For this work, we employed ResNet-50 because for the given amount of data, it gave the best performance. We employed Inception-V3 as it has been used by researchers before as well on related tasks. Inception-ResNet-V2 was implemented as given by C. Szegedy et al.¹⁹ Hyperparameter values used in these algorithms are given in Table III.

4.4 State-of-the-art Methods for Comparison

There are only a handful of machine learning approaches reported in literature for wet-blue leather classification. Also, these learning approaches do not publicly share their source code or executable programs that can be used for reproducing their results for comparative evaluation. Therefore, in this work, we compare the performance of the proposed method with contemporary interest point based machine learning techniques and benchmark deep learning methods discussed above. The main motivation for choosing these techniques is their widespread use in literature for similar defect classification problems. We briefly discuss the use of selected techniques in relevant defect detection problems.

Hassanin et al. applied SURF features to classify defects on a printed circuit board (PCB).²⁰ Zheng D. used Harris corner features for classification of patterns in fabric design.²¹ Shang et. al. used inception-v3 with transfer learning to classify and recognize rail surface defects.²² Wen et. al. used ResNet-50 with transfer learning for fault diagnosis.²³ Shahin et. al. has applied ensemble strategy on skin lesion classification using Inception-v3 and ResNet-50 as an ensemble algorithm.²⁴

Therefore, in this work, we compare the classification performance of the proposed CNN based ensemble with the state-of-the-art feature descriptors including SURF by Bay et al.,²⁰ FAST by Rosten and Drummond²¹ and BRISK points proposed by Leutenegger et al.²² employed in a classification framework. We also employ the well-known Harris corner points algorithm by Harris and Stephens²³ as a baseline descriptor for comparison purpose. These descriptors are employed in a well-known bag-of-keypoints based classification framework²⁴ (with multiclass SVM as the classifier) for a fair comparison. In addition, we employ ResNet, inception-V3 and Inception-ResNet-V2 as benchmark deep learning based methods and VGG-16 as a baseline deep learning method.

5 Results

All the algorithms were validated on 328 images during the training process. Before giving the images as an input to the model, all these images were pre-processed. The hyper-parameters used for training are given in Table III. The classification results of the proposed method are presented in Figure 3. It can be observed from the confusion matrices that the proposed Inception-V3+ResNet-50 architecture obtained a high percentage of correct predictions with a high precision and has the ability to robustly identify almost all irregular features in general. This is also confirmed by the ROC curves and the high AUC values as evident in Figure 3. The high AUC values also exhibit the ability of the proposed method to adapt to various applications where different threshold values may be required.

Table III

Hyper-parameter values used in algorithms

Name	Hyper-Parameter Value
Global average pooling	Replaced fully connected layer
Output layer	Activation: Softmax
Number of epochs	20
Batch size	4, 12
Optimization method	SGD & Adam (Learning rate = 0.001)

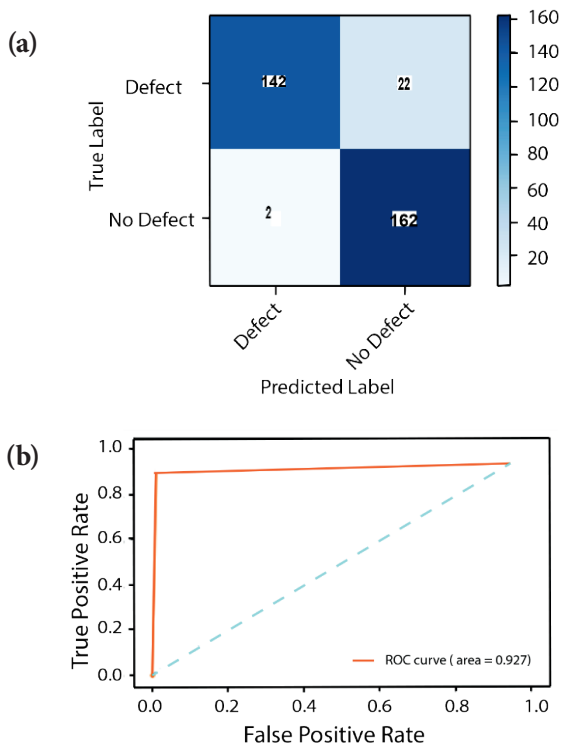


Figure 3. Confusion matrices and ROC curves for the proposed method. (a) confusion matrix (b) ROC curve

Table IV

Comparison with the state-of-the-art methods in terms of classification accuracy. T Acc stands for Training Accuracy, Val Acc for Validation Accuracy and Test Acc for Test Accuracy.

Serial #	Model	Training Acc (%)	Validation Acc (%)	Test Acc (%)
1	SURF1	94.44	71.67	83.33
2	FAST16	81.67	81.67	73.33
3	BRISK9	94.44	60.00	75.00
4	Harris6	95.00	63.33	76.67
5	InceptionV3+ResNet-50	97.64	96.29	92.68

5.1 Comparison with Descriptors Based Machine Learning Methods

In this section, we evaluate the efficacy of the proposed method in comparison to the state-of-the-art feature descriptors based learning methods (discussed in Section 4.4) in terms of classification accuracy, precision, recall, F1-score and AUC. Table IV compares the performance of the proposed methods with the state-of-the-art methods in terms of classification accuracy on the training, validation and test sets. The proposed Inception-V3+ResNet-50 method outperforms all other methods in terms of training accuracy as well as its generalization ability on unseen images. The state-of-the-art methods obtained high training accuracy but in general failed to generalize well on unseen examples in the validation and test sets. The SURF²⁰ and the FAST²¹ methods performed at par on test data with better generalization ability as compared with the BRISK²² and the Harris¹⁷ descriptors. It is evident from these results that the proposed CNN based method is more suitable as compared with the state-of-the-art machine learning methods due to its robust prediction ability.

It can be observed from Table V that the proposed Inception-V3+ResNet-50 method outperforms all other compared methods in terms of precision, recall, F1-score and AUC. The SURF method

Table V

Comparison of methods in terms of precision, recall, F1-score and AUC.

Serial #	Model	Precision	Recall	F1-score	AUC
1	SURF1	0.86	0.80	0.83	0.90
2	FAST16	0.68	0.87	0.76	0.66
3	BRISK9	0.80	0.67	0.73	0.78
4	Harris6	0.83	0.67	0.74	0.76
5	InceptionV3+ResNet-50	0.93	0.93	0.93	0.927

Table VI
Comparison of models in terms of accuracy, transfer learning, batch normalization,
batch size using Global Average Pooling and image size of 500×375.

Serial #	Image Size	Model Name	Train Accuracy (%)	Validation Accuracy (%)	Test Accuracy (%)	Optimizer	GAP	Transfer Learning	Scratch	Batch Normalization	Batch Size	AUC
1	500×375	VGG-16	62.5	0	50	SGD	✓	✗	✓	✗	4	50
2	500×375	VGG-16	63.08	0	50	Adam	✓	✓	✗	✗	4	50
3	500×375	VGG-16	67.54	0	50	Adam	✓	✗	✓	✗	4	50
4	500×375	ResNet-50	99.33	97.31	89.76	Adam	✓	✗	✓	✓	4	89.8
5	500×375	ResNet-50	98.08	99.27	89.47	SGD	✓	✗	✓	✓	4	89.5
6	500×375	ResNet-50	100	94.65	53.54	Adam	✓	✓	✗	✗	4	53.5
7	500×375	ResNet-50	100	99.63	90.85	SGD	✓	✓	✗	✗	4	90.7
8	500×375	Inception-v3	95.48	94.23	65.74	SGD	✓	✗	✓	✓	4	65.7
9	500×375	Inception-v3	95.58	98.85	90.15	SGD	✓	✓	✗	✗	12	90.1
10	500×375	Inception-v3	90.19	40.38	33.85	Adam	✓	✗	✓	✗	12	33.9
11	500×375	Inception-v3	99.04	97.31	74.4	Adam	✓	✓	✗	✗	12	74.4
12	500×375	Inception-ResNet-V2	97.88	49.23	24.8	Adam	✓	✗	✓	✓	12	24.9
13	500×375	Inception-ResNet-V2	98.56	99.61	74.8	SGD	✓	✓	✗	✗	12	74.9
14	500×375	Inception-ResNet-V2	99.9	100	54.72	Adam	✓	✓	✗	✗	4	54.8
15	500×375	Inception-ResNet-V2	97.5	96.15	76.77	Adam	✓	✗	✓	✗	4	76.8
16	500×375	Inception-V3+Inception-ResNet-V2	99.45	94.84	91.52	Adam	✓	✓	✗	✗	4	91.5
17	500×375	Inception-V3+ResNet-50	97.64	96.29	92.68	SGD	✓	✓	✗	✗	4	92.7

generalizes well on the test data as quantified by its AUC which is in agreement with its accuracy. Despite competitive accuracy, the FAST method did not generalize well in terms of AUC. This suggests that although the FAST method can obtain correct predictions, it may not be much more reliable in different applications, where different thresholds are to be set for the classifier. The results of the Harris and the BRISK features are also in line with their accuracy scores.

5.2 Comparison with Deep Learning Based Methods

To harness the true performance of the CNN based methods, we experimented with multiple optimization functions and found that the Adam and the Stochastic Gradient Descent (SGD) optimizers are best suited for our problem. We also experimented with transfer learning (with ImageNet¹² weights) in comparison to training from scratch. To aid training from scratch batch normalization was also employed. Some important conclusions drawn from the results in Table V include: 1) The Adam optimizer was found to be the preferred choice for all the networks, 2) Transfer learning from ImageNet weights was found to be more useful in comparison to training from scratch, 3) Batch normalization could not help in improving the results when training the networks from scratch.

Two key observations from our experiments in Table VI are that: 1) knowledge learned from ImageNet transfers better to the task at hand as compared with training from scratch. 2) Inception-V3 and ResNet-50 stand out as compared with other architectures in terms of their performance on leather defect classification. Therefore, when performing our ensembling experiments, we used pre-trained architectures on ImageNet. Also, we select the Inception-V3+ResNet-50 as our proposed ensemble architecture in comparison and compare it with other ensemble approaches. The proposed Inception-V3+ResNet-50 architecture outperformed all other CNN variants in terms of all three accuracy measures when trained using the SGD optimizer in a transfer learning setting. It is also evident that the proposed architecture could be trained with the largest batch size owing to its reduced parameters and compactness. The proposed architecture takes only 1.3 milli seconds to classify an image of resolution 500×375. Surprisingly, VGG-16²⁵ could not perform well on this task. This result suggests that only sixteen layers of the VGG-16 network are shallow to learn effective representations for the leather classification task. ResNet-50 learned effective representations and exhibited the second best performance in terms of the accuracy measures. Interestingly, it performed slightly better than the Inception-ResNet-V2 architecture in terms of validation and test accuracies.

6 Class Activations Maps (CAM)

The important region(s) in images utilized by the CNN to predict the class label of an input image can be visualised in several ways, such as gradient descent class activation mappings and global average pooling class activation mappings, etc. In order to interpret the output decision made by any of the CNN architectures investigated in this study, we employ class activation mappings to produce heat maps, which show regions of high importance that influenced the classification output of the method. Figure 4 shows the class activation maps of the proposed method in comparison to other deep learning approaches. In Figure 4, yellow and pink colors are used to represent the regions of high importance according to a particular classifier. Ideally, the regions of high importance should be abnormal surfaces for correct prediction of classes. It is evident from Figure 4 that the proposed method considers the abnormal surfaces (defects) to classify the defective images. Apart from the proposed method only Inception-V3 is able to recognize the abnormal regions to a considerable extent. Otherwise, all other compared methods are not able to focus on important regions potentially leading to misclassifications.

7 Conclusion

Automated visual inspection of leather in an industrial setting has gained considerable attention recently. Numerous machine learning approaches have been proposed in the past, however, convolutional neural networks based approaches are scarce. In this work, we propose an ensemble convolutional neural network for visual inspection of wet-blue leather. We also present a new dataset of high-resolution leather images. Our proposed technique was able to outperform more than 10 deep learning and machine learning based methods in terms of both test accuracy and AUC score. Our model was able to obtain test accuracy of 92.68% and AUC score of 92.7%. Despite, it's competitive performance, the proposed method would require adaptation for real-time application, which includes fine tuning on video data. In the future, an important direction is to develop a system that can classify leather data in a real-world industrial setting. Another important future direction is to adapt the current system to classify multiple defect types. Finally, the

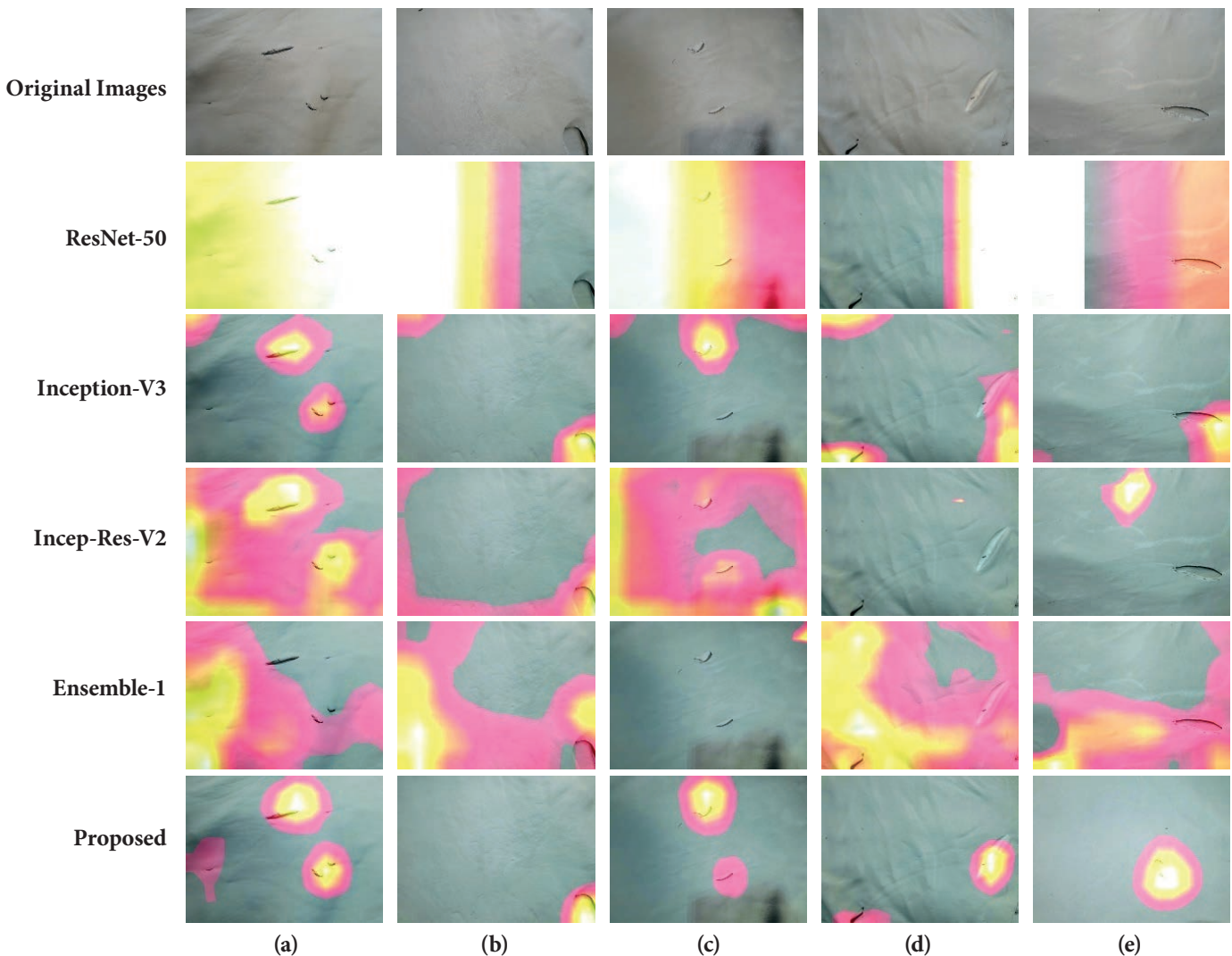


Figure 4. Class activations maps of ResNet-50, Inception-v3, Inception-ResNet-v2 (Incep-Res-V2), Inception-v3 & Inception-ResNet-v4 (Ensemble-1), and Inception-v3 and ResNet-50 (Proposed), respectively.

development of such systems that can characterize various defect types in terms of their properties can potentially lead to artificial intelligence based automated quality grading of leather samples.

Acknowledgment

This work was supported by NZ Leather and Shoe Research Association (LASRA*), Palmerston North, New Zealand through the Ministry of Business, Innovation and Employment (MBIE) grant number LSRX1801.

References

1. C. Koch, K. Georgieva, V. Kasireddy, B. Akinci, and P. Fieguth, "A review on computer vision based defect detection and condition assessment of concrete and asphalt civil infrastructure," *Adv. Eng. Informatics*, vol. 29, no. 2, pp. 196–210, 2015, doi: <https://doi.org/10.1016/j.aei.2015.01.008>.
2. H. Zheng, L. X. Kong, and S. Nahavandi, "Automatic inspection of metallic surface defects using genetic algorithms," *J. Mater. Process. Technol.*, vol. 125–126, pp. 427–433, 2002, doi: [https://doi.org/10.1016/S0924-0136\(02\)00294-7](https://doi.org/10.1016/S0924-0136(02)00294-7).
3. H. Y. T. Ngan, G. K. H. Pang, and N. H. C. Yung, "Automated fabric defect detection—A review," *Image Vis. Comput.*, vol. 29, no. 7, pp. 442–458, 2011, doi: <https://doi.org/10.1016/j.imavis.2011.02.002>.
4. S. Vaidya, P. Ambad, and S. Bhosle, "Industry 4.0 – A Glimpse," *Procedia Manuf.*, vol. 20, pp. 233–238, 2018, doi: <https://doi.org/10.1016/j.promfg.2018.02.034>.
5. M. Egmont-Petersen, D. de Ridder, and H. Handels, "Image processing with neural networks—a review," *Pattern Recognit.*, vol. 35, no. 10, pp. 2279–2301, 2002, doi: [https://doi.org/10.1016/S0031-3203\(01\)00178-9](https://doi.org/10.1016/S0031-3203(01)00178-9).
6. Khwaja Muinuddin Chisti Mohammed, Srinivas Kumar S, Prasad G, Defective texture classification using optimized neural network structure, *Pattern Recognition Letters*, Volume 135, 2020, Pages 228–236, ISSN 0167-8655, <https://doi.org/10.1016/j.patrec.2020.04.017>.
7. J. Deng, J. Liu, C. Wu, T. Zhong, G. Gu and B. W. -K. Ling, "A Novel Framework for Classifying Leather Surface Defects Based on a Parameter Optimized Residual Network," in *IEEE Access*, vol. 8, pp. 192109–192118, 2020, doi: 10.1109/ACCESS.2020.3032164.
8. M. Aslam, T. M. Khan, S. S. Naqvi, G. Holmes, and R. Naffa, "Ensemble Convolutional Neural Networks with Knowledge Transfer for Leather Defect Classification in Industrial Settings," *IEEE Access*, vol. 8, pp. 198600–198614, 2020.
9. H. Robbins and S. Monro, "A stochastic approximation method," *Ann. Math. Stat.*, pp. 400–407, 1951.
10. D. P. Kingma and J. Ba, "Adam: {A} Method for Stochastic Optimization," 3rd International Conference on Learning Representations, {ICLR} 2015, 2015, <http://arxiv.org/abs/1412.6980>.
11. S. Mannor, D. Peleg, and R. Rubinfeld, "The cross entropy method for classification," in *Proceedings of the 22nd international conference on Machine learning*, 2005, pp. 561–568.
12. J. Deng, W. Dong, R. Socher, L. Li, Kai Li, and Li Fei-Fei, "ImageNet: A large-scale hierarchical image database," in *2009 IEEE Conference on Computer Vision and Pattern Recognition*, 2009, pp. 248–255.
13. C. Szegedy, V. Vanhoucke, S. Ioffe, J. Shlens, and Z. Wojna, "Rethinking the Inception Architecture for Computer Vision," in *2016 IEEE Conference on Computer Vision and Pattern Recognition (CVPR)*, 2016, pp. 2818–2826. https://github.com/keras-team/keras-applications/blob/master/keras_applications/inception_v3.py.
14. M. Oquab, L. Bottou, I. Laptev, and J. Sivic, "Is object localization for free? - Weakly-supervised learning with convolutional neural networks," in *2015 IEEE Conference on Computer Vision and Pattern Recognition (CVPR)*, 2015, pp. 685–694.
15. B. Zhou, A. Khosla, A. Lapedriza, A. Oliva, and A. Torralba, "Learning Deep Features for Discriminative Localization," in *2016 IEEE Conference on Computer Vision and Pattern Recognition (CVPR)*, 2016, pp. 2921–2929.
16. P. O. Pinheiro and R. Collobert, "From image-level to pixel-level labeling with Convolutional Networks," in *2015 IEEE Conference on Computer Vision and Pattern Recognition (CVPR)*, 2015, pp. 1713–1721.
17. T. Durand, N. Thome, and M. Cord, "WELDON: Weakly Supervised Learning of Deep Convolutional Neural Networks," in *2016 IEEE Conference on Computer Vision and Pattern Recognition (CVPR)*, 2016, pp. 4743–4752. https://github.com/keras-team/keras-applications/blob/master/keras_applications/vgg16.py.
18. K. He, X. Zhang, S. Ren, and J. Sun, "Deep Residual Learning for Image Recognition," in *2016 IEEE Conference on Computer Vision and Pattern Recognition (CVPR)*, 2016, pp. 770–778. https://github.com/keras-team/keras-applications/blob/master/keras_applications/resnet50.py.
19. C. Szegedy, S. Ioffe, V. Vanhoucke, and A. A. Alemi, "Inception-v4, inception-ResNet and the Impact of Residual Connections on Learning," in *Proceedings of the Thirty-First AAAI Conference on Artificial Intelligence*, 2017, pp. 4278–4284. https://github.com/keras-team/keras-applications/blob/master/keras_applications/inception_resnet_v2.py.
20. H. Bay, A. Ess, T. Tuytelaars, and L. Van Gool, "Speeded-Up Robust Features (SURF)," *Comput. Vis. Image Underst.*, vol. 110, no. 3, pp. 346–359, 2008.
21. E. Rosten and T. Drummond, "Fusing points and lines for high performance tracking," in *Tenth IEEE International Conference on Computer Vision (ICCV'05)*, 2005, vol. 2, pp. 1508–1515.
22. S. Leutenegger, M. Chli, and R. Y. Siegwart, "BRISK: Binary Robust invariant scalable keypoints," in *2011 International Conference on Computer Vision*, 2011, pp. 2548–2555, doi: 10.1109/ICCV.2011.6126542.
23. C. Harris and M. Stephens, "A combined corner and edge detector," in *In Proc. of Fourth Alvey Vision Conference*, 1988, pp. 147–151.
24. G. Csurka, C. R. Dance, L. Fan, J. Willamowski, and C. Bray, "Visual categorization with bags of keypoints," in *In Workshop on Statistical Learning in Computer Vision, ECCV*, 2004, pp. 1–22.
25. K. Simonyan and A. Zisserman, "Very Deep Convolutional Networks for Large-Scale Image Recognition," 3rd International Conference on Learning Representations, {ICLR} 2015, 2015, <http://arxiv.org/abs/1409.1556>.

Lifelines

Qian Zhang received her Master's degree in 2020 from School of Materials Science and Engineering at Zhengzhou University, Zhengzhou, China, majoring in leather chemistry and engineering. Her research focuses on the clean production in leather making.

Jie Liu received his PhD degree in 2007 from Institute of Mechanics, Chinese Academy of Sciences, Beijing, China. He currently is an associate professor at School of Materials Science and Engineering at Zhengzhou University, Zhengzhou, China. From 2016 to 2017, he worked as a visiting scientist at ERRC, USDA in Cheng-Kung Liu's group. His current research interests focus on green composite materials based on natural polymers and their applications in packaging, biomedical and environmental fields.

Xiumin Li received his PhD degree in 2017 from Hirosaki University, Aomori, Japan. He is working for Zhengzhou University as an associate professor at School of Materials Science and Engineering, Zhengzhou, China. His research interests include the electro-catalyst materials and nanostructure engineering. He has published more than 50 papers and co-authored 1 book in the field of nanostructured material.

Hui Liu received his PhD degree in 2020 from Zhengzhou University, Zhengzhou, China. His research focuses on the mechanism and application of simplified clean production of ecological leather with biological enzymes.

Yadi Hu is a PhD candidate of School of Materials Science and Engineering at Zhengzhou University, majoring in the materials physics and chemistry. Her research focuses on the degradation mechanism of modern and historical leathers under the effect of storage environmental conditions.

Keyong Tang received his PhD degree in 1998 from Sichuan University, Chengdu, China. He is working for Zhengzhou University as a professor at School of Materials Science and Engineering, Zhengzhou, China. His research interests include the leather structure and properties. He has published more than 100 papers, co-authored 4 books and edited 1 book in the field of leather chemistry and engineering.

Xueru Guo received her B.S. degree in Environmental Engineering in Shaanxi University of Science & Technology in 2017. Now she is undertaking her M.D. degree in Biomass Chemistry and Engineering at Sichuan University. Her research focuses on chrome-free tanning technology.

Yue Yu, see *JALCA* 115, 190, 2020.

Ya-nan Wang, see *JALCA* 112, 258, 2017.

Bi Shi, see *JALCA* 99, 220, 2004.

Qiao Xia received his Bachelor's degree from Chengdu University of TCM 2019. He is currently studying for a master's degree with Prof. Zongcai Zhang at Sichuan University. His research interests are in leather chemistry and engineering.

Zongcai Zhang received his Doctor's degree in leather chemistry and engineering from Sichuan University in 2005. His research mainly focuses on the cleaner technology and development of fine chemicals for leather and fur.

Meina Zhang received her Master's degree from Sichuan University 2020. He is currently studying for a Doctor's degree at University of Liverpool. Her research concentration is in chemistry.

Yingxuan Wang received her Bachelor's degree from Xi'an University of Architecture and Technology 2019. She is currently studying for a Master's degree with Prof. Zongcai Zhang at Sichuan University.

Hong Dai received her doctorate degree in leather chemistry and engineering from Sichuan University in 2006. Her research mainly focuses on analysis and testing of leather and fur.

Masood Aslam received the B.S. degree in electrical engineering from The University of Faisalabad, Faisalabad, Pakistan, in 2013, and the M.S. degree in electrical engineering from FASTNUCES, Islamabad, Pakistan, in 2018. He is currently working as Research Associate with the Visual Computing Technology (VC-Tech) Lab, Islamabad. Before joining VC-Tech, he worked as a Research Assistant with FAST-NUCES. His research interests include computer vision and image processing.

Tariq M. Khan (Member, IEEE) received the Ph.D. degree from Macquarie University, Sydney, Australia. He is currently working as a Research Fellow at Deakin University. At CUI, he also serving as a Head of the Image and Video Processing Research Group (IVPRG). He has over ten years of research, and teaching experience in universities including CUI, Macquarie University, and UET Taxila, Pakistan. He was a recipient of several awards including iMQRES scholarship, Macquarie University Postgraduate Research Student Support (PRSS) travel grants and SRGP. He is interested in both digital image processing (with an emphasis on medical imaging) and machine learning. His research interests include most aspects of image enhancement, pattern recognition, and image analysis.

He has published 40 journals and 22 conference papers in well-reputed journals and conferences e.g. IEEE Transactions on Image Processing, Pattern Recognition, IEEE Access, Expert Systems with Applications, JRTIP, ICIAR, VCIP, and DICTA. His research has received research funding from Effat University, HEC Pakistan, MBIE New Zealand, and KSA International Collaboration Grant over \$1M in past years.

Syed Saud Naqvi received the B.Sc. degree in computer engineering from the COMSATS Institute of Information Technology, Islamabad, Pakistan, and the M.Sc. degree in electronic engineering from the University of Sheffield, U.K., in 2005 and 2007, respectively, and the Ph.D. degree from the School of Engineering and Computer Science, Victoria University of Wellington, New Zealand, in 2016. He is currently working as an Assistant Professor with the COMSATS Institute of Information Technology Islamabad, Pakistan. His research interests include saliency modeling, medical image analysis, scene understanding, and deep learning methods for image analysis.

Geoff Holmes received the degree in applied science from Kingston University, in 1986, and the H.N.D. degree in leather technology from the University of Northampton's Institute for Creative Leather Technologies, in 1989. He is a Leather Technologist. He has over 30 years' experience in the leather industry in various production and technical roles, and for the last 14 years has been involved in research at the New Zealand Leather and Shoe Research Association (LASRA). He is the current LASRA Director.

Rafea Naffa received the Ph.D. degree in biochemistry from the School of Fundamental Sciences, Massey University, in 2017. He is currently a Scientist with the Leather and Shoe Research Association, Palmerston North, New Zealand. He has published more than 18 peer-reviewed articles since 2017, including six method articles. He is also studying the extraction, purification, and characterization of collagen from different animal species for several applications. His research focuses on the analysis of collagen in skins and hides where he developed several analytical methods for the separation and quantitation of collagen crosslinks and advanced glycation end products using LC-MS.

Celebrating
75 Years
1941-2016

UNION
Specialties, Inc.

**The power of water-based
polyurethane technology**

3 Malcolm Hoyt Dr. Newburyport, MA 01950, USA. Certified ISO 9001:2015
Tel: +1 978-465-1717 Fax: +1 978 465-4194 E-mail: union@unionspecialtiesinc.com

www.unionspecialtiesinc.com



Stahl's innovations driven by sustainability

With the rise of both electric and self-driving, cars are becoming quieter and anti-squeak and rattle materials are becoming increasingly important. At the same time, improved anti-stain performance is required, because of the current trend for pale-colored car seats. Therefore, we have developed Stay Clean. This low-VOC coating technology protects pale-colored leather and vinyl surfaces against common stains, such as dye from jeans, spilled coffee and dirt. Our solution also makes surfaces low-squeak, which is a great asset as global research has shown that a squeaking car interior is one of the biggest annoyances among car owners. Another trend in car interior is the popularity of matt surfaces. Therefore, we have developed PolyMatte®. This non-squeaking solution provides a luxurious feel to the finished article in combination with flexibility and scratch and abrasion resistance. Our portfolio contains many products, varying from beamhouse products, tanning systems to finishes,

duller concentrates, crosslinkers and thickeners to leveling agents, defoamers, colorants and hand modifiers. Our most sustainable option is Green PolyMatte®, which is based on rapeseed oil (20%) instead of crude oil-derived intermediates. If you would like to know what our Stahl solutions for automotive can do for your business, please visit www.stahl.com or contact us at: alexander.campbell@us.stahl.com.

If it can be imagined, it can be created



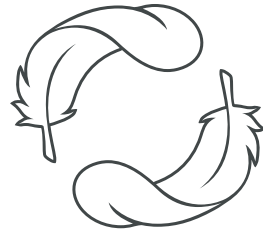
Stay Clean



Low-VOC



PolyMatte®



C O L D M i l l i n g



Smooth Leather
Milling



Obituary

Raymond Anthony Hart Jr. passed away March 30, 2021 at Kaplan Family Hospice House in Danvers, Massachusetts. He was 86 years old.

Born in Swampscott, Massachusetts on March 19, 1935, he grew up in Massachusetts and North Carolina, the son of Raymond and Margaret (Reppucci) Hart. He attended Lynn English High School, and after graduation he joined the Army. He served six years in the USAR as a Combat Engineer, rising to Sergeant.

Raymond studied chemistry at Tufts University, graduating in 1956 to pursue a career in the leather industry, following in his father's footsteps. As a Leather Chemist he worked for A.C. Lawrence, Ciba Geigy, John Flynn and Sons, and Ciba of Switzerland, developing modern tanning processes in the US, Canada, and Europe. He joined The American Leather Chemists Association in 1965 and became a life member in 2006. He served the Association as a member of the Alsop Selection Committee in 1993.

Raymond married Barbara Frances Schmermond of Pine Orchard, Connecticut in 1959. They raised their family in Marblehead, Massachusetts, spending summers in Tuftonboro, NH. Raymond enjoyed coaching Marblehead Youth Basketball and Football, and CYO Basketball at Star of the Sea Church.

Upon his retirement, he and Bobi moved to their favorite spot in Tuftonboro, making new friends at the Rotary Club and Katharine

Drexel Parish. They traveled the world, hosted family gatherings, and spent time volunteering. Ray took great pleasure in teaching the art of fly-tying at summer camps, delivering Meals on Wheels, and supporting the 48 Hours of Food program in Carroll County. You could usually find Ray fishing, tying flies, listening to old jazz, and talking with friends on the dock. Despite losing his eyesight later in life, he continued to pursue his love of fly fishing with his family and friends.

Raymond was predeceased by his wife, Bobi, the love of his life, in 2019. They were married 60 years.

Raymond leaves two sons, Raymond A. Hart III of Merrimack, NH, and Patrick M. Hart and his wife, Leah of Marblehead, MA. He leaves one grandson, Raymond A. Hart IV and his wife, Jessica of Hooksett, NH, a granddaughter Claudia Hart, two great-grandsons, Ethan Douglas and Whittaker Steele, and his dog Raegan.

The family wishes to thank everyone who reached out to bring joy into Ray's life, especially the Friendly Visitors from St. Katharine Drexel Parish in Alton, NH, his friends from Lakeside, and the Central NH VNA. Donations in Ray's name may be made to St. Katharine Drexel Parish, PO Box 180, Wolfeboro NH 03894.

To sign an online guest book, leave a message or condolences, go to: www.baker-gagnefuneralhomes.com

INDEX TO ADVERTISERS

ALCA Annual Meeting	<i>Inside Back Cover</i>
Buckman Laboratories.	<i>Inside Front Cover</i>
Chemtan.	<i>Back Cover</i>
Chemtan.	146
Erretre	183
Stahl	182
Union Specialties Inc	181



**116th ALCA
ANNUAL CONVENTION
Change of Date:
June 21–24, 2022
Eaglewood Resort & Spa
Itasca, IL**

**Featuring the 61st John Arthur Wilson Memorial Lecture
By Randy Johnson, President and CEO
of GST AutoLeather
Title: Road Ahead**

Tentative Schedule

Tuesday, June 21

Golf Tournament, Opening Reception and Dinner

Wednesday, June 22

***John Arthur Wilson Memorial Lecture
All Day Technical Sessions, Fun Run
Reception and Dinner, Activities - Bowling, Pool,
Darts and an Open Bar***

Thursday, June 23

***All Day Technical Sessions, Annual Business Meeting
Activities Awards Luncheon
Social Hour, ALCA Awards Banquet***

***Visit us at www.leatherchemists.org for full details
under Annual Convention as they become available***

Sometimes Safety Begins with Reflection



Chemtan®
Reflect V-100



 **CHEMTAN**

Tel: (603) 772-3741 • www.CHEMTAN.com